

000 001 002 003 004 005 006 007 008 009 010 011 012 013 014 015 016 017 018 019 020 021 022 023 024 025 026 027 028 029 030 031 032 033 034 035 036 037 038 039 040 041 042 043 044 045 046 047 048 049 050 051 052 053 GOGO: GROUP-WISE GRANULARITY-ORDERED CODEC FOR STABLE AND EFFICIENT SPEECH GENERATION

Anonymous authors

Paper under double-blind review

ABSTRACT

Current speech language models require their core component, the speech codec, to discretize continuous speech signals into tokens that not only capture high-level cues for autoregressive modeling but also preserve sufficient acoustic details for perceptual quality. To address this need, we propose Gogo, a group-wise granularity-ordered codec that quantizes each group of frames into tokens arranged from coarse to fine, where coarse tokens encode high-level abstractions and fine tokens progressively recover low-level details. Building on the granularity-ordering property of Gogo, we introduce GogoSpeech, a two-stage speech language model that performs speech generation by first constructing a coarse speech backbone at an extremely low token rate and then enriching the backbone with fine-grained acoustic details. Considering the inherently non-uniform information distribution in speech signals, we further design a Group Relative Policy Optimization (GRPO)-trained token allocator that adaptively allocates token budgets to groups based on group-wise complexity. Experimental results demonstrate that Gogo delivers state-of-the-art reconstruction performance across most metrics at a token rate of 47. Moreover, evaluations on zero-shot text-to-speech tasks show that GogoSpeech enables efficient generation by adaptively reducing the average token rate, and attains state-of-the-art results in long-form speech generation.

1 INTRODUCTION

Large language models (LLMs) such as the GPT series (Brown et al., 2020; OpenAI, 2024) have demonstrated remarkable capabilities across diverse text-based tasks. Their success has inspired growing efforts to extend the LLM paradigm to the speech modality, leading to the development of speech language models (SLMs) capable of understanding and generating spoken language (Ye et al., 2025b; Fang et al., 2025; Défossez et al., 2024). A common pipeline for SLMs first discretizes continuous speech into sequences of tokens via an audio codec, then models both text and speech tokens in an autoregressive framework. The effectiveness of this approach hinges critically on the codec’s ability to produce tokens that concurrently contain high-level cues (*e.g.*, content, semantics, and structural attributes) for autoregressive modeling (Ye et al., 2025a) and sufficient acoustic details (*e.g.*, low-level acoustic fluctuations) for perceptual quality preservation.

Conventional audio codecs, originally designed for compression and transmission, adopt a frame-wise quantization scheme (Kleijn et al., 2021; Valin et al., 2012; Défossez et al., 2022). While this enables high-fidelity reconstruction, its strong locality bias limits the codec’s ability to capture high-level cues needed by SLMs. To address this limitation, recent works have augmented codecs with self-supervised representations (Défossez et al., 2024; Zhang et al., 2024; Li et al., 2025) or automatic speech recognition (ASR) features (Du et al., 2024b; Jo et al., 2025; Zeng et al., 2025) to explicitly inject high-level linguistic and semantic information into the quantization process. However, the fundamental frame-wise quantization paradigm remains unbroken, inherently limiting the ability to learn high-level information. Besides, little attention has been given to the non-uniform information distribution in speech (Dieleman et al., 2021; Voran, 2024). Current approaches generally allocate one same bitrate to all segments, which leads to redundant coding and low generation efficiency, especially in less complex segments like silence where a low coding rate would suffice.

To address the aforementioned limitations, we redesign both the codec and SLM framework. As depicted in Figure 1, we first propose Gogo, a group-wise granularity-ordered codec that processes

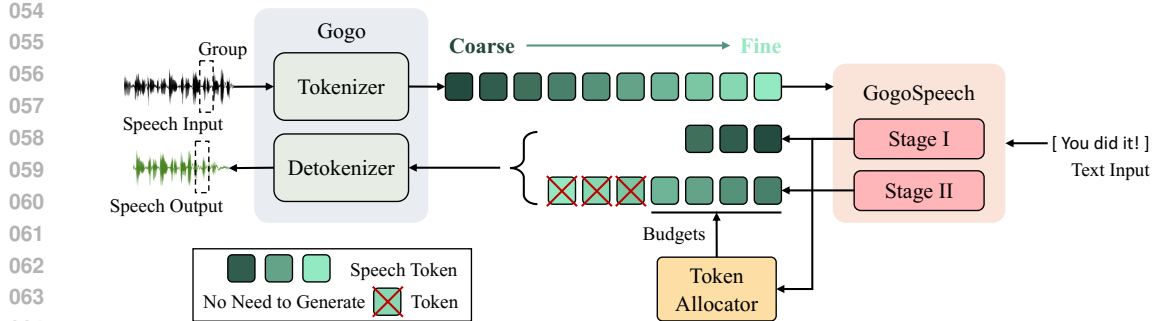


Figure 1: System overview. The shading of a token reflects the granularity of the information it encodes. **The token allocator allocates different token budgets to different groups within the same utterance based on their complexity.** Only one group is plotted for simplicity. Best viewed in color.

contiguous frames as groups and generates tokens in a coarse-to-fine order, where coarse tokens capture high-level information and fine tokens are used to progressively restore low-level acoustic details. Building on the granularity-ordering property of Gogo, we develop GogoSpeech, a two-stage SLM for speech generation. In the first stage, a high-level speech backbone, which serves as a coarse indicator of the target speech, is predicted at a extremely low feature rate (around 14 Hz). This reduced feature rate enhances the stability of autoregressive prediction and mitigates error accumulation (Arora et al., 2022; He et al., 2021). In the second stage, fine-grained details are incrementally recovered conditioned on the speech backbone. The feature rate in the second stage is restored to a standard level to ensure high-fidelity synthesis with precise details. To further enhance efficiency, we propose a Group Relative Policy Optimization (GRPO)-trained (Shao et al., 2024) token allocator that dynamically assigns token budgets to every group based on its complexity, thereby aligning computational resources with the non-uniform information density of speech signals.

Our main contributions in this work are fivefold: (1) proposing a new speech codec, namely Gogo, featuring group-by-group and granularity-ordered tokenization that better addresses the representational requirements of SLMs; (2) constructing a new speech language model, namely GogoSpeech, enabling staged speech generation from high-level abstractions to fine acoustic details; (3) developing a GRPO-trained token allocator that optimizes efficiency and quality by aligning token budgets with group-wise complexity; (4) conducting reconstruction experiments to show that Gogo achieves superior performance compared to state-of-the-art codecs; (5) performing experiments on text-to-speech (TTS) to show that GogoSpeech achieves better performance with higher stability and efficiency. Demo samples can be found at <https://anonymous.4open.science/w/gogo>.

2 RELATED WORK

2.1 NEURAL AUDIO CODECS

Modern neural audio codecs are predominantly based on the VQ-GAN framework (Esser et al., 2021), which integrates an encoder, a vector quantizer, and a decoder into an end-to-end system. Pioneering works such as SoundStream (Zeghidour et al., 2021) and EnCodec (Défossez et al., 2022) employ residual vector quantization (RVQ) together with carefully designed discriminators to improve perceptual fidelity. DAC (Kumar et al., 2023) further enhances codebook utilization by performing code lookup in a low-dimensional space using cosine similarity rather than Euclidean distance. To improve compatibility with SLMs, recent studies have explored injecting linguistic or semantic information into the quantization process. One line of work leverages self-supervised speech representations from models such as HubERT (Hsu et al., 2021), WavLM (Chen et al., 2022), and w2v-BERT (Chung et al., 2021). For example, SpeechTokenizer (Zhang et al., 2024) distills semantic teacher representations into the first stage of RVQ, while Mimi (Défossez et al., 2024) transfers semantic information into a single-stage quantizer to decouple acoustic reconstruction from semantic coding. Another line of research integrates ASR features into codec training. Notably, S^3 tokenizer (Du et al., 2024a) partitions the encoder of a pretrained SenseVoice ASR model (An et al.,

108 2024) and inserts a quantization layer between its two halves. Despite recent advancements, the
 109 frame-wise quantization paradigm remains unchanged. Its inherent locality bias limits the codec’s
 110 ability to learn high-level cues, which are essential for stable autoregressive modeling in SLMs.
 111

112 2.2 SPEECH LANGUAGE MODELS

113 Generative speech language modeling extends the LLM paradigm to the speech modality by mod-
 114 eling discrete speech tokens produced by neural audio codecs or clustering methods such as k-
 115 means. Early works such as GSLM (Lakhotia et al., 2021) and SpeechGPT (Zhang et al., 2023) di-
 116 rectly train language models on speech tokens, enabling the generation of natural-sounding speech.
 117 VALL-E (Wang et al., 2023) adopts an autoregressive model to generate the first token and a non-
 118 autoregressive model to predict residual tokens from EnCodec. To address the trade-off between
 119 high-fidelity reconstruction and effective autoregressive modeling, AudioLM (Borsos et al., 2023)
 120 introduces a hierarchical modeling framework that first generates semantic tokens and then refines
 121 them with acoustic tokens. In general, acoustic tokens are designed to encode speech at a low bi-
 122 trate while preserving as much information as possible, whereas semantic tokens are learned from
 123 self-supervised speech models to capture phonetic or semantic representations that facilitate speech
 124 comprehension (Guo et al., 2025b). This hierarchical paradigm has inspired numerous follow-up
 125 works, including AudioPaLM (Rubenstein et al., 2023), Moshi (Défossez et al., 2024), and TTS-
 126 Llama (Shen et al., 2025). While the hierarchical approach improves stability and controllability,
 127 the semantic modeling stage in existing methods typically operates at the same token rate as the
 128 acoustic modeling stage, which is substantially higher than the token rate used in the text modality.
 129

130 2.3 ADAPTIVE BITRATE IN NEURAL CODECS

131 The non-uniform information density of speech signals makes constant-bitrate codecs inherently in-
 132 efficient. SNAC (Siuzdak et al., 2024) extends RVQ to operate at multiple temporal resolutions, yet
 133 the bitrate remains fixed across different speech regions. Acoustic BPE (Shen et al., 2024) applies
 134 the byte-pair encoding (BPE) algorithm (Devlin et al., 2019) to speech tokens, reducing sequence
 135 length and increasing token correlation. More recently, VRVQ (Chae et al., 2025) introduces a
 136 variable-bitrate strategy into RVQ, allowing the number of quantizers per frame to be adaptively
 137 determined from a predicted importance map. Similarly, TFC (Zhang et al., 2025) dynamically allo-
 138 cates frame rates to different regions according to temporal entropy. However, these variable-bitrate
 139 codecs do not explicitly couple bitrate variation with reconstruction quality for joint optimization,
 140 and their effectiveness in generative tasks within the SLM framework remains underexplored.
 141

142 3 METHODS

143 3.1 GOGO

144 The proposed Gogo, as shown in Figure 2, comprises three main components: an encoder for learn-
 145 ing speech representations, a flow-based generative model (Lipman et al., 2023; Tong et al., 2024)
 146 for mel-spectrogram reconstruction, and a vocoder for converting spectrograms into waveforms.
 147 Additionally, Gogo integrates an ASR module and an autoregressive (AR) prior (Wang et al., 2025;
 148 Yang et al., 2025) to enhance the suitability of the learned speech tokens for downstream generation.
 149

150 3.1.1 WORKFLOW

151 Given an input waveform w , we first extract its mel-spectrogram $x \in \mathbb{R}^{n_f \times d}$, where n_f denotes
 152 the number of frames and d the number of mel bins. The spectrogram is then partitioned along
 153 the temporal axis into multiple non-overlap groups $x^i \in \mathbb{R}^{g \times d}$, where g denotes the group size,
 154 $i \in [1, n_g]$ denotes the group index, and $n_g = \lceil \frac{n_f}{g} \rceil$ denotes the total number of groups. The
 155 last group is zero-padded if necessary. Subsequently, each group is concatenated with n_q learnable
 156 queries $q^i \in \mathbb{R}^{n_q \times d}$, which yields $z^i \in \mathbb{R}^{(g+n_q) \times d}$. Incorporating queries into quantization has been
 157 explored in ALMTokenizer (Yang et al., 2025), TiTok (Yu et al., 2024), and FlexTok (Bachmann
 158 et al., 2025). The extended sequences z^i are encoded by Transformer (Vaswani et al., 2017) encoder,
 159 after which the x^i part is discarded and finite scalar quantization (FSQ) (Mentzer et al., 2024) is
 160 applied to the positions corresponding to the learnable queries, producing speech token indices $s^i \in$
 161

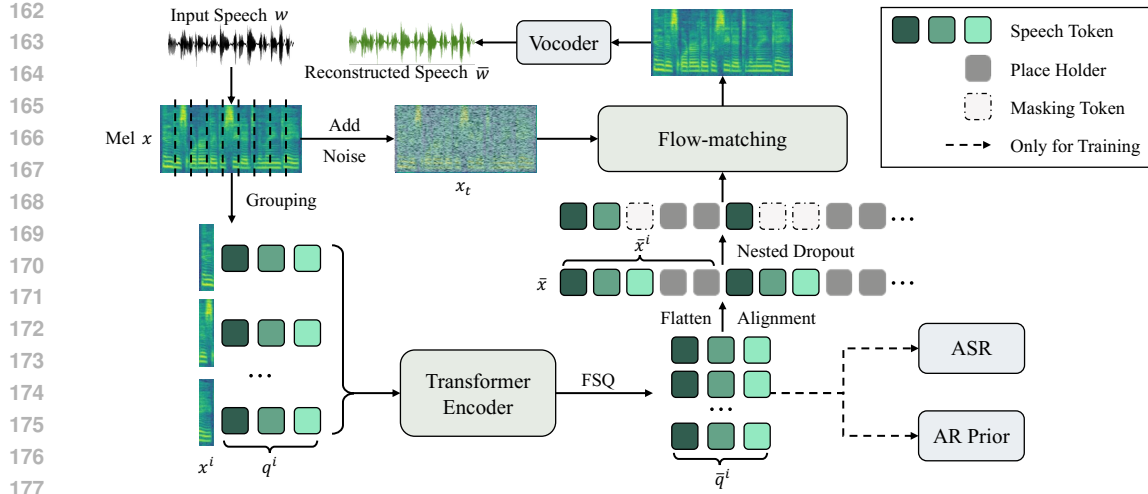


Figure 2: Architecture of Gogo. Here the group size g is set to 5 and the number of speech queries n_q assigned to each group is set to 3 for demonstration. Best viewed in color.

\mathbb{R}^{n_q} and their corresponding embeddings $\bar{q}^i \in \mathbb{R}^{n_q \times d_h}$, where d_h denotes the hidden dimension. Formally, the tokenization workflow in Gogo is given by:

$$\begin{aligned} x &= \text{Mel}(w), \\ x^1, x^2, \dots, x^{n_g} &= \text{Grouping}(x), \\ z^i &= \text{Cat}(x^i, q^i), \\ \bar{q}^i, s^i &= \text{FSQ}(\text{Encoder}(z^i)), \end{aligned} \tag{1}$$

where $\text{Mel}(\cdot)$ denotes the mel extraction operation, $\text{Grouping}(\cdot)$ denotes the grouping operation, and $\text{Cat}(\cdot)$ denotes the concatenation operation. We omit the batch dimension for clarity. In practice, the effective batch size for the encoder is n_g times the number of speech samples loaded in a batch.

For reconstruction, \bar{q}^i are first padded with $(g - n_q)$ placeholder tokens to match the original group length g , resulting in aligned features $\bar{x}^i \in \mathbb{R}^{g \times d_h}$. All groups' \bar{x}^i are concatenated along the time axis to generate $\bar{x} \in \mathbb{R}^{n_f \times d_h}$, which is then fed into a flow-matching model to predict the mel-spectrogram. The final waveform \bar{w} is recovered using a pretrained Vocos (Siuzdak, 2023) vocoder. Formally, the reconstruction workflow in Gogo is given by:

$$\begin{aligned} \bar{x}^i &= \text{Cat}(\bar{q}^i, \text{Placeholders}), \\ \bar{x} &= \text{Cat}(\bar{x}^1, \bar{x}^2, \dots, \bar{x}^{n_g}), \\ \bar{w} &= \text{Vocoder}(\text{Flow}(\bar{x})). \end{aligned} \tag{2}$$

3.1.2 TRAINING OBJECTIVES

Gogo leverages conditional flow matching (CFM) (Lipman et al., 2023), which extends the framework of continuous normalizing flows (Chen et al., 2018) to learn a time-dependent vector field that transports a simple prior distribution, e.g., the standard normal distribution, to the distribution of the mel-spectrograms conditioned on the features \bar{x} . Given a mel-spectrogram x_1 and a Gaussian noise $x_0 \sim \mathcal{N}(0, I)$, we first interpolate between them and produce a noisy spectrogram $x_t = (1 - t)x_0 + tx_1$ using a flow time $t \sim \mathcal{U}(0, 1)$. The conditional vector field for this linear interpolation is $v(x_0, x_1, t) = \partial x_t / \partial t = x_1 - x_0$. The flow-matching model, parameterized by θ , takes (x_t, \bar{x}, t) as input and predicts a velocity vector $v_\theta(x_t, \bar{x}, t)$. Formally, the CFM objective is defined as a simple vector field regression loss:

$$\mathcal{L}_{\text{CFM}} = \mathbb{E}_{t, p(x_0), q(x_1)} \left[\|v_\theta(x_t, \bar{x}, t) - v(x_0, x_1, t)\|_2^2 \right]. \tag{3}$$

We further introduce two auxiliary modules, AR prior and ASR module, to encourage the speech queries to capture temporal dependencies and linguistic information within each group, respectively.

216 The corresponding training objectives, \mathcal{L}_{AR} and \mathcal{L}_{ASR} , are formally defined in Appendix B. Finally,
 217 the objective for training Gogo can be written as:
 218

$$\mathcal{L}_{\text{Gogo}} = \lambda_{\text{CFM}} \mathcal{L}_{\text{CFM}} + \lambda_{\text{AR}} \mathcal{L}_{\text{AR}} + \lambda_{\text{ASR}} \mathcal{L}_{\text{ASR}}, \quad (4)$$

220 where λ_{CFM} , λ_{AR} , and λ_{ASR} are coefficients employed to balance different loss components.
 221

222 3.1.3 GRANULARITY ORDERING

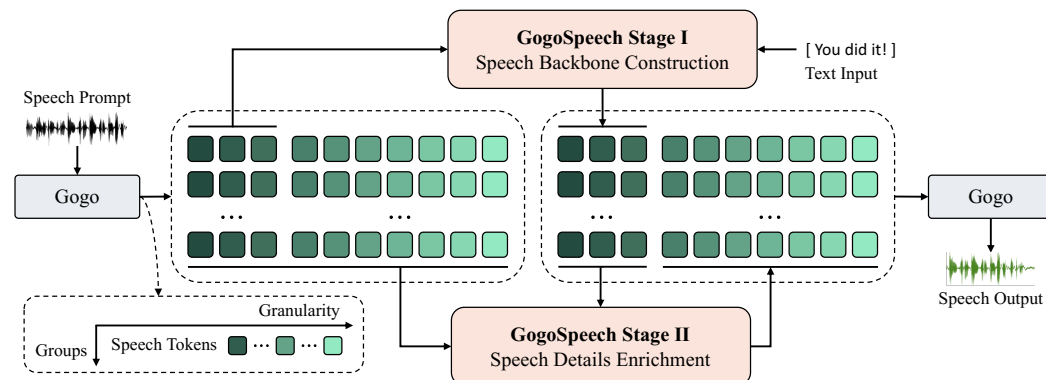
224 To enforce a coarse-to-fine ordering in the learned speech queries q^i and tokens s^i , we introduce two
 225 techniques: nested dropout (Rippel et al., 2014) and loss balancer.

226 **Nested dropout** randomly drops tokens in a nested fashion during training. Specifically, we uni-
 227 formly sample the number of tokens to retain, $n_k \in \{1, \dots, n_q\}$, and replace the last $(n_q - n_k)$
 228 tokens with masking tokens m . This mechanism drives Gogo to prioritize encoding high-level ab-
 229 stractions and essential structural attributes into the earlier coarse tokens to minimize $\mathcal{L}_{\text{Gogo}}$ to the
 230 greatest extent, while deferring the challenging and fluctuating details to the later fine tokens. Since
 231 later tokens are rarely preserved and receive fewer gradient updates, we further introduce a re-
 232 weighting mechanism for compensation. Concretely, the gradient of the j -th speech token is scaled
 233 by $w_j = 0.5 / (1 - (j-1)/n_q)$, assigning larger weights to tokens with fewer updates and vice versa.
 234 Details of the re-weighting implementation are provided in Appendix A.

235 **Loss balancer** is utilized to adjust the loss coefficients λ_{CFM} and λ_{ASR} , further ensuring that the
 236 learned speech tokens are organized in a coarse-to-fine manner. Specifically, when n_k is small, the
 237 model should emphasize \mathcal{L}_{ASR} so that coarse tokens encode richer linguistic content. Conversely,
 238 when n_k is large, \mathcal{L}_{CFM} should dominate to ensure that fine tokens capture more acoustic details.
 239 Let λ_{max} and λ_{min} denote the maximum and minimum weighting coefficients, respectively. The loss
 240 balancer adaptively adjusts λ_{CFM} and λ_{ASR} as follows:

$$\lambda_{\text{CFM}} = \lambda_{\text{min}} + \frac{(n_k - 1)(\lambda_{\text{max}} - \lambda_{\text{min}})}{n_q - 1}, \quad \lambda_{\text{ASR}} = \lambda_{\text{max}} - \frac{(n_k - 1)(\lambda_{\text{max}} - \lambda_{\text{min}})}{n_q - 1}. \quad (5)$$

244 3.2 GOGOSPEECH



260 Figure 3: Architecture of GogoSpeech. Gogo encodes the speech prompt into speech tokens, which
 261 serve as input to GogoSpeech for generating the target speech tokens. The target speech tokens are
 262 transformed into waveform by Gogo. For visualization, the number of speech queries n_q in each
 263 group is set to 10 and the speech backbone is defined as the first 3 speech tokens of each group.

264 3.2.1 STAGE I: SPEECH BACKBONE CONSTRUCTION

265 Stacking all s^i yields a 2D token matrix $\mathbf{S} \in \mathbb{R}^{n_g \times n_q}$. The speech backbone is defined as the first b
 266 tokens of each group, *i.e.*, $\mathbf{S}_{:,1:b} \in \mathbb{R}^{n_g \times b}$, which contains the high-level cues of the speech signal.
 267 As shown in Figure 3, given the input text $y = (y_1, \dots, y_L)$ and the backbone of speech prompt
 268 $\mathbf{S}_{:,1:b}$, the autoregressive model in Stage I generates the backbone of target speech $\tilde{\mathbf{S}}_{:,1:b} \in \mathbb{R}^{\tilde{n}_g \times b}$

270 group by group, where \tilde{n}_g denotes the number of groups in the target speech. Let $\Gamma(\cdot)$ denote the
 271 operation that flattens a token matrix into a sequence. The objective of Stage I is to minimize the
 272 negative log-likelihood over the target speech backbone:
 273

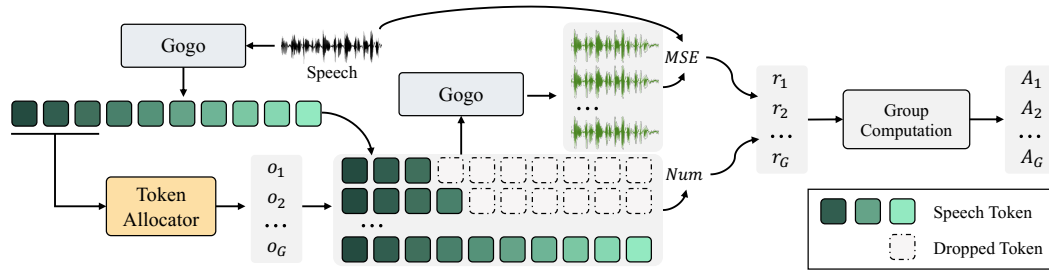
$$274 \quad \mathcal{L}_{\text{stage1}} = - \sum_{i=1}^{\tilde{n}_g} \sum_{t=1}^b \log P(\tilde{\mathbf{S}}_{i,t} \mid y, \Gamma(\mathbf{S}_{:,1:b}), \Gamma(\tilde{\mathbf{S}}_{1:i-1,1:b}), \tilde{\mathbf{S}}_{i,1:t-1}) \quad (6)$$

277 3.2.2 STAGE II: SPEECH DETAILS ENRICHMENT

278 In Stage II, GogoSpeech progressively enriches the speech backbone predicted in Stage I by adding
 279 fine-grained acoustic details group by group. For the i -th group of the target speech, the auto-
 280 regressive model in Stage II generates the fine tokens $\tilde{\mathbf{S}}_{i,b+1:n_q}$ conditioned on all tokens of the input
 281 speech prompt \mathbf{S} , all tokens of the previously generated groups $\tilde{\mathbf{S}}_{1:i-1,:}$, and the speech backbone
 282 of the current group $\tilde{\mathbf{S}}_{i,1:b}$. The training objective for Stage II is given by:
 283

$$284 \quad \mathcal{L}_{\text{stage2}} = - \sum_{i=1}^{\tilde{n}_g} \sum_{t=b+1}^{n_q} \log P(\tilde{\mathbf{S}}_{i,t} \mid \Gamma(\mathbf{S}), \Gamma(\tilde{\mathbf{S}}_{1:i-1,:}), \tilde{\mathbf{S}}_{i,1:t-1}) \quad (7)$$

287 3.3 TOKEN ALLOCATOR



299 Figure 4: GRPO-trained token allocator. Throughout the GRPO training, the Gogo is kept frozen.
 300

301 To improve the efficiency of speech generation, we want to allocate more tokens to acoustically
 302 complex groups while assigning fewer tokens to simpler ones, such as silence. To enable such adapt-
 303 ive allocation, we design a token allocator that receives the backbone of each group, $\tilde{\mathbf{S}}_{i,1:b}$, as input
 304 and outputs a budget $\xi_i \in \{0, 1, \dots, n_q - b\}$, indicating the number of fine tokens to be generated for
 305 that group in GogoSpeech Stage II. The skipped unnecessary fine tokens are replaced with masking
 306 tokens m . The cooperation between the token allocator π_ω and GogoSpeech is formulated as:
 307

$$308 \quad \xi_i = \pi_\omega(\tilde{\mathbf{S}}_{i,1:b}) \in \{0, 1, \dots, n_q - b\}, \quad (8)$$

$$309 \quad \tilde{\mathbf{S}}_{i,b+1:b+\xi_i} = \arg \max_u \prod_{j=b+1}^{b+\xi_i} p(u_j \mid y, \Gamma(\mathbf{S}), \Gamma(\tilde{\mathbf{S}}_{1:i-1,:}), \tilde{\mathbf{S}}_{i,1:j-1}), \quad \tilde{\mathbf{S}}_{i,b+\xi_i+1:n_q} = m. \quad (9)$$

310 As shown in Figure 4, the token allocator is trained from scratch using a slightly modified GRPO
 311 technique (Shao et al., 2024). Given that the output space of the allocator is relatively small, compris-
 312 ing $(n_q - b + 1)$ discrete allocation choices, we enumerate all possible outputs (o_1, o_2, \dots, o_G) , cor-
 313 responding to using from b to n_q tokens for reconstructing the input speech. The resulting $(n_q - b + 1)$
 314 reconstructed samples are employed to compute the group scores.
 315

316 We adopt two reward metrics, including \mathcal{R}_n which penalizes the number of tokens utilized for re-
 317 construction, and \mathcal{R}_d which penalizes the distance between the input and reconstructed speech. This
 318 joint reward encourage the allocator to learn allocation strategies that achieve high reconstruc-
 319 tion fidelity while minimizing the number of tokens consumed. The rewards \mathcal{R}_n and \mathcal{R}_d , and the entire
 320 reward \mathcal{R} are defined as follows:
 321

$$322 \quad \mathcal{R}_n = -\text{Num}(\bar{x}), \quad \mathcal{R}_d = -\mathbb{E} \left[\|\text{Mel}(w) - \text{Mel}(\bar{w})\|_2^2 \right], \quad (10)$$

$$323 \quad \mathcal{R} = \lambda_n \mathcal{R}_n + \lambda_d \mathcal{R}_d, \quad (11)$$

324 where $\text{Num}(\bar{x})$ denotes the number of speech tokens used to generate \bar{w} , λ_n and λ_d are coefficients
 325 used to balance the two reward terms. After obtaining the reward for each allocation choice, the
 326 advantage is calculated using group relative advantage estimation (Shao et al., 2024):
 327

$$328 \quad \mathcal{A}_j = \frac{\mathcal{R}_j - \text{mean}(\mathcal{R})}{\text{std}(\mathcal{R})}. \quad (12)$$

330 Since the token allocator is initialized from scratch, we omit the KL penalty term used in the original
 331 GRPO framework. The allocator π_ω is then optimized by maximizing the following objective:
 332

$$333 \quad \mathcal{J}_{\text{GRPO}} = \mathbb{E}_{o_j \sim \pi_\omega(o|\tilde{\mathbf{S}}_{i,1:b})} \left[\frac{1}{G} \sum_{j=1}^G \pi_\omega(o_j|\tilde{\mathbf{S}}_{i,1:b}) \mathcal{A}_j \right]. \quad (13)$$

337 4 EXPERIMENTAL SETUP

339 4.1 IMPLEMENTATION DETAILS

341 We extract 100-dimensional log mel-filterbank features from audio resampled to 24 kHz, using a
 342 hop length of 256 and a window size of 1024, resulting in a feature rate of approximately 94 Hz. We
 343 set the group size to $g = 20$, and allocate $n_q = 10$ speech queries per group. Therefore, the token
 344 rate of Gogo is computed as $n_q \times (94/g) = 47$ Hz. The speech backbone is defined as the first $b = 3$
 345 tokens of each group. Thus the token rate of backbone is about 14 Hz. Both Stage I and Stage II of
 346 GogoSpeech are initialized from the LLaMA (Grattafiori et al., 2024), with the vocabulary expanded
 347 to include speech tokens. A pretrained Vocos (Siuzdak, 2023) is employed to convert the generated
 348 spectrograms into waveforms. Please refer to Appendix C for more detailed model configuration.

349 During training, we empirically set the weight of loss \mathcal{L}_{AR} to $\lambda_{\text{AR}} = 0.06$ and amplify the gradient
 350 of the AR prior by a factor of 50 to ensure effective updates. The coefficients for the losses \mathcal{L}_{ASR}
 351 and \mathcal{L}_{CFM} are dynamically adjusted using the loss balancer defined in Eq. 5, with $\lambda_{\text{min}} = 0.2$ and
 352 $\lambda_{\text{max}} = 1.8$. For training the token allocator via GRPO, we set the reward coefficients $\lambda_n = 0.2$ and
 353 $\lambda_d = 1.0$ to balance the trade-off between token efficiency and reconstruction quality. Additional
 354 hyperparameters, training schedules, and inference configurations are provided in Appendix D.

355 4.2 DATASETS

357 We train both Gogo, GogoSpeech, and the token allocator on the Emilia dataset (He et al., 2024),
 358 a large-scale and diverse in-the-wild speech corpus designed for multilingual speech generation.
 359 In this work, we use its English subset, which contains approximately 50K hours of transcribed
 360 speech covering a diverse set of speakers, acoustic characteristics, and background conditions. For
 361 evaluating the reconstruction quality of Gogo, we adopt the LibriTTS test-clean set (Zen et al., 2019)
 362 with 4,837 samples in total. To assess the zero-shot speech generation capability of GogoSpeech,
 363 we use the Seed-TTS test-en set (Anastassiou et al., 2024), which consists of 1,000 samples drawn
 364 from Common Voice dataset (Ardila et al., 2019). All speech samples are resampled to 24 kHz.

365 4.3 BASELINES AND EVALUATION METRICS

367 We compare Gogo against multiple codec baselines, including EnCodec (Défossez et al., 2022),
 368 DAC (Kumar et al., 2023), SpeechTokenizer (Zhang et al., 2024), Mimi (Défossez et al., 2024),
 369 SNAC (Siuzdak et al., 2024), WavTokenizer (Ji et al., 2025), MagiCodec (Song et al., 2025), X-
 370 codec2 (Ye et al., 2025b), TAAE (Parker et al., 2025), and DualCodec (Li et al., 2025). All baseline
 371 results are obtained using their official checkpoints. Details of compared codecs see Appendix E.

372 We compare GogoSpeech with TTS baselines, including FireRedTTS-1S (Guo et al., 2025a), F5-
 373 TTS Chen et al. (2025), XTTS-v2 (Casanova et al., 2024), Llasa (Ye et al., 2025b), CosyVoice 2 (Du
 374 et al., 2024b), and VoiceCraft (Peng et al., 2024). More details can be found in Appendix F.

376 For evaluation, we employ both objective and subjective metrics. For objective assessment, we adopt
 377 UT-MOS (Saeki et al., 2022), DNS-MOS (Reddy et al., 2022), and Perceptual Evaluation of Speech
 Quality (PESQ) (Rix et al., 2001) to quantify perceptual quality and speech distortion. Speech

378
 379 Table 1: Comparison between different codec models on the LibriTTS test-clean set. Bold values
 380 indicate the best for each token rate. TPS and FPS denote the number of tokens and frames per
 381 second, respectively. #CB denotes the number of codebook employed in each model.
 382

Model	TPS	FPS	#CB	UT MOS	DNS MOS	STOI	PESQ WB	PESQ NB	SIM	WER
Ground Truth	-	-	-	4.13	3.83	1.00	4.64	4.55	1.00	5.86
DAC	600	75	8	3.78	3.75	0.99	3.52	3.85	0.98	6.10
EnCodec	600	75	8	3.13	3.56	0.94	2.74	3.36	0.97	6.24
DAC	150	75	2	1.94	3.27	0.85	1.53	1.95	0.90	10.81
EnCodec	150	75	2	1.57	3.20	0.85	1.54	1.92	0.91	8.98
SpeechTokenizer	150	50	3	3.10	3.56	0.85	1.47	1.86	0.90	7.23
Mimi	150	12.5	12	3.88	3.77	0.94	2.67	3.22	0.95	6.54
SNAC	82	47	3	3.80	3.84	0.91	2.23	2.75	0.91	7.47
DAC	75	75	1	1.33	2.97	0.76	1.18	1.45	0.81	30.06
EnCodec	75	75	1	1.24	2.69	0.78	1.21	1.45	0.77	33.15
WavTokenizer	75	75	1	4.11	3.65	0.92	2.43	2.96	0.90	8.34
Mimi	75	12.5	6	3.54	3.69	0.90	2.01	2.53	0.90	7.65
SpeechTokenizer	50	50	1	1.31	3.09	0.68	1.11	1.28	0.67	9.18
MagiCodec	50	50	1	4.21	3.96	0.93	2.55	3.18	0.86	7.45
X-codec2	50	50	1	4.17	3.90	0.92	2.45	3.07	0.83	6.40
TAAE	50	25	2	4.27	3.89	0.91	2.14	2.82	0.87	8.18
DualCodec	50	25	2	4.05	3.80	0.89	2.02	2.58	0.89	6.54
Mimi	50	12.5	4	3.16	3.62	0.86	1.64	2.10	0.87	9.24
Gogo	47	47	1	4.19	3.99	0.92	2.59	3.26	0.91	6.35

403
 404 intelligibility is measured using Short-Time Objective Intelligibility (STOI) (Taal et al., 2010) and
 405 Word Error Rate (WER). In addition, speaker similarity (SIM) is calculated to evaluate the accuracy
 406 of speaker identity preservation. For subjective evaluation, we employ the Similarity Mean Opinion
 407 Score (SMOS) and Comparative MOS (CMOS) to assess speaker similarity and relative naturalness,
 408 respectively. Detailed definitions for each metric are provided in Appendix G.
 409

410 5 EXPERIMENTAL RESULTS

411 5.1 CODEC COMPARISON

412 We compare our Gogo with a range of existing codecs, and the results are summarized in Table 1.
 413 Despite operating at a relatively low token rate of 47 tokens per second, Gogo achieves superior
 414 performance across multiple metrics compared to codecs operating at 50 tokens per second. DAC
 415 and EnCodec achieve the best overall performance when operating at a high token rate of 600, with
 416 the exception of UT-MOS and DNS-MOS. However, their performance degrades significantly as
 417 the token rate is reduced. Notably, Gogo attains UT-MOS and DNS-MOS scores that even surpass
 418 the ground-truth recordings, which we attribute to the generative nature of Gogo’s flow-matching
 419 decoder, enabling enhanced perceptual quality and improved noise robustness.
 420

421 5.2 EFFECTIVENESS OF GROUP-WISE QUANTIZATION FOR AUTOREGRESSIVE MODELING

422 To evaluate whether group-wise quantization better supports downstream AR modeling, we train a
 423 naive autoregressive model to perform AR prediction over speech token sequences, which are con-
 424 structed by collecting the j -th token from each group in Gogo, where $j \in [1, n_q]$. For the frame-wise
 425 baseline, we remove the grouping operation in Gogo and replace FSQ with a 10-level RVQ, follow-
 426 ing the standard frame-wise quantization scheme. Each RVQ layer generates a frame-level token
 427 sequence that encodes the residual information left by all preceding layers. Each sequence is mod-
 428 eled autoregressively, and perplexity is reported as an indicator of modeling difficulty. Additional
 429 experimental details and perplexity computation are provided in Appendix I.
 430

432
433
434
435
436Table 2: Perplexity of autoregressive modeling on speech tokens produced by different quantization schemes. Column headers specify the source of speech tokens, denoting their positions within each group for group-wise quantization or their corresponding RVQ layer for frame-wise quantization. The boldface denotes the best result. \dagger indicates frame-wise quantization with single-layer VQ.437
438
439
440
441

Scheme	1	2	3	4	5	6	7	8	9	10
Frame-wise \dagger	247.8	-	-	-	-	-	-	-	-	-
Frame-wise	2.3	25.9	84.4	114.9	189.2	261.2	441.8	442.0	727.8	691.4
Group-wise	0.9	8.5	42.0	96.9	169.5	201.6	204.1	221.9	229.6	228.3

442
443
444
445
446
447
448
449
450

The perplexity results are summarized in Table 2. Group-wise quantization consistently yields lower perplexity across all granularities than frame-wise quantization, suggesting that the group-wise tokens produced by Gogo are more autoregressive-friendly and capture temporal dependencies more effectively. We can also see that coarse tokens yield substantially lower perplexity than fine tokens in both quantization schemes, confirming that fine-grained acoustic details are more challenging for AR models to predict. These findings further motivate the two-stage design of GogoSpeech, where a high-level speech backbone is generated first, followed by fine-grained detail enrichment.

451
452

5.3 WHAT DO GRANULARITY-ORDERED TOKENS ENCODE?

453
454
455
456
457
458

To gain deeper insight into the behavior of group-wise granularity-ordered quantization, we conduct probing experiments on Gogo’s tokens at different granularities to examine the type of information each token encodes. We probe these tokens using a diverse set of acoustic, prosodic, and linguistic features. The probing task is formulated as a regression problem, where the mean squared error reported by the probing model is used as an indicator of each token’s representational capacity. More details of the probing setup are provided in Appendix H.

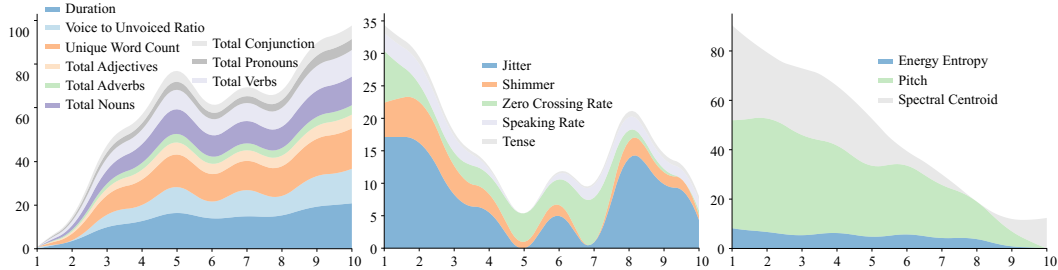
459
460
461
462
463
464
465
466
467
468469
470
471
472
473

Figure 5: Performance of granularity-ordered tokens across multiple feature prediction tasks. Results are visualized as stacked area charts, where the x-axis denotes token positions within each group and the y-axis indicates the normalized prediction loss relative to the maximum loss for each feature. A higher value corresponds to greater loss and thus lower predictive performance.

474
475
476
477
478
479
480
481

The probing results, presented in Figure 5, reveal a clear progression of information across token granularities. Specifically, the first three tokens primarily capture global and high-level information, such as total duration, voiced-to-unvoiced ratio, word count, and linguistic content. Tokens in the middle range predominantly encode prosodic attributes, including speaking rate, jitter, and shimmer. Finally, the last three tokens are responsible for capturing detailed acoustic information, such as pitch, energy, and spectral centroid. These findings confirm that Gogo’s group-wise quantization organizes tokens in a coarse-to-fine manner, allowing high-level linguistic and prosodic cues to be modeled with fewer tokens while reserving fine tokens for detailed acoustic reconstruction.

482
483
484
485

5.4 ZERO-SHOT TTS COMPARISON

We compare GogoSpeech with several state-of-the-art TTS baselines, and the results are summarized in Table 3. In objective evaluations, GogoSpeech achieves the highest SIM and competitive WER

486
 487 Table 3: Comparison between different TTS models on the Seed-TTS test-en set. The boldface de-
 488 notes the best result, the underline denotes the second best. **The Real-Time Factor (RTF)** is computed
 489 by averaging the inference time of a 47-character sentence over 100 trials on an H100 GPU.

Model	Objective					Subjective	
	SIM	WER	SIM [†]	WER [†]	RTF	SMOS	CMOS
Ground Truth	0.734	2.143	0.809	2.037	-	4.752	0.000
F5-TTS (Chen et al., 2025)	0.647	1.830	0.716	<u>1.812</u>	0.184[‡]	4.173	+1.730
XTTS-v2 (Casanova et al., 2024)	0.463	3.248	0.490	2.292	<u>0.208</u>	2.426	-0.961
Llasa-8B-250k (Ye et al., 2025b)	0.574	2.970	0.629	5.947	<u>0.944</u>	3.297	+0.882
CosyVoice 2 (Du et al., 2024b)	0.654	2.380	0.701	2.324	<u>0.549</u>	<u>4.331</u>	+1.638
FireRedTTS-1S (Guo et al., 2025a)	0.660	<u>2.170</u>	0.705	2.129	<u>0.506</u>	4.247	+1.634
VoiceCraft (Peng et al., 2024)	0.470	7.556	0.360	10.25	<u>1.248</u>	2.965	-0.751
GogoSpeech (47 Hz)	0.667	2.394	0.725	1.788	0.535	4.381	+1.832
w/ Allocator (47 Hz → 36 Hz)	0.662	2.469	<u>0.717</u>	1.845	0.455	4.253	+1.587

501 [†] All target speeches corresponding to the same prompt speech are concatenated, and only constructed sam-
 502 ples longer than 10s are retained to evaluate the stability of systems in long speech generation.

503 [‡] F5-TTS is fully non-autoregressive, while the other systems include autoregressive decoding.

506 compared to the leading systems. For long-form speech generation, it further attains the best SIM
 507 and WER, demonstrating the effectiveness of the two-stage design in enhancing generation stability.
 508 In subjective evaluations, GogoSpeech achieves the best SMOS and CMOS scores, confirming its
 509 ability to preserve speaker identity while maintaining strong intelligibility and overall quality.

511 5.5 EFFECTIVENESS OF TOKEN ALLOCATOR

513 We further evaluate the effectiveness of the proposed token allocator by comparing GogoSpeech
 514 with and without adaptive token allocation. The results are presented in the last two rows of Table 3.
 515 With the token allocator, GogoSpeech generates on average only 36 tokens per second of speech,
 516 compared to 47 tokens without adaptive allocation. The token allocator significantly reduces the
 517 computational cost of speech generation and incurs only a marginal performance degradation in
 518 both objective and subjective scores. **As for inference efficiency, F5-TTS is fully non-autoregressive**
 519 **and therefore naturally achieves the lowest RTF. Among the AR systems, GogoSpeech with the**
 520 **token allocator is only slower than XTTS-v2, yet it delivers substantially stronger performance.**
 521 These results demonstrate that the token allocator achieves a favorable trade-off between generation
 522 efficiency and speech quality. Please refer to Appendix L for visualization of adaptive allocation.

523 6 LIMITATIONS

525 Despite its strong performance, our system has several limitations. First, placeholder tokens in the
 526 flow-matching decoder can occasionally introduce artifacts. Second, Gogo operates at a token rate
 527 of 47 Hz, which is higher than the low-bitrate codecs of 25 Hz. Finally, GogoSpeech is built on
 528 Llama-3.2-1B-Instruct, and its scalability to larger language models requires further investigation.

530 7 CONCLUSION

532 In this paper, we present Gogo, a group-wise granularity-ordered codec, and GogoSpeech, a two-
 533 stage speech language model. Specifically, Gogo produces autoregressive-friendly tokens for each
 534 speech group, arranged in order from coarse to fine. Built upon Gogo, GogoSpeech performs speech
 535 generation by first constructing a high-level speech backbone, then enriching it with fine-grained
 536 details. Furthermore, we proposed a GRPO-trained token allocator that adaptively allocates token
 537 budgets based on group-wise complexity, significantly reducing the number of tokens required for
 538 synthesis without sacrificing perceptual quality. Extensive experiments on speech reconstruction and
 539 zero-shot text-to-speech demonstrate that Gogo achieves superior performance compared to state-
 of-the-art codecs, and GogoSpeech delivers high-quality, stable, and efficient speech generation.

540
541
ETHICS STATEMENT

542 This work introduces a speech generation model capable of producing highly human-like speech
 543 and supporting zero-shot voice cloning. While these capabilities advance the state of the art, they
 544 also present potential risks, including misuse for misinformation, impersonation, or other forms of
 545 harmful synthetic audio. Our research is intended solely for legitimate scientific purposes. To pro-
 546 mote responsible deployment, we advocate transparent disclosure of synthetic speech, appropriate
 547 access control, and careful monitoring of downstream use. We are also exploring complementary
 548 safeguards such as speech watermarking and deepfake detection to enhance the traceability of gen-
 549 erated audio. We encourage the community to adopt similar precautions to ensure that advances in
 550 generative speech technology are used ethically and for societal benefit.

551 This study also involves subjective listening evaluations for assessing the quality of synthesized
 552 speech. All participants were fully informed of the purpose and procedure of the listening task, and
 553 their participation was entirely voluntary. Consent was obtained prior to the evaluation. Participants
 554 were asked to complete the evaluation in a quiet environment to ensure reasonable listening condi-
 555 tions. The study did not collect any personal or identifying information, and no sensitive data or
 556 high-risk procedures were involved.

557
558 **REFERENCES**

559
 560 Keyu An, Qian Chen, Chong Deng, Zhihao Du, Changfeng Gao, Zhifu Gao, Yue Gu, Ting He,
 561 Hangrui Hu, Kai Hu, et al. Funaudiollm: Voice understanding and generation foundation models
 562 for natural interaction between humans and llms. *arXiv preprint arXiv:2407.04051*, 2024.

563 Philip Anastassiou, Jiawei Chen, Jitong Chen, Yuanzhe Chen, Zhuo Chen, Ziyi Chen, Jian Cong,
 564 Lelai Deng, Chuang Ding, Lu Gao, et al. Seed-tts: A family of high-quality versatile speech
 565 generation models. *arXiv preprint arXiv:2406.02430*, 2024.

566
 567 Rosana Ardila, Megan Branson, Kelly Davis, Michael Henretty, Michael Kohler, Josh Meyer,
 568 Reuben Morais, Lindsay Saunders, Francis M Tyers, and Gregor Weber. Common voice: A
 569 massively-multilingual speech corpus. *arXiv preprint arXiv:1912.06670*, 2019.

570 Kushal Arora, Layla El Asri, Hareesh Bahuleyan, and Jackie Chi Kit Cheung. Why exposure bias
 571 matters: An imitation learning perspective of error accumulation in language generation. In
 572 *Findings of the Association for Computational Linguistics: ACL 2022*, pp. 700–710, 2022.

573 Roman Bachmann, Jesse Allardice, David Mizrahi, Enrico Fini, Oğuzhan Fatih Kar, Elmira Amir-
 574 loo, Alaaeldin El-Nouby, Amir Zamir, and Afshin Dehghan. Flextok: Resampling images into
 575 1d token sequences of flexible length. In *Forty-second International Conference on Machine
 576 Learning*, 2025.

577
 578 James Betker. Better speech synthesis through scaling. *arXiv preprint arXiv:2305.07243*, 2023.

579
 580 Zalán Borsos, Raphaël Marinier, Damien Vincent, Eugene Kharitonov, Olivier Pietquin, Matt Shar-
 581 ifi, Dominik Roblek, Olivier Teboul, David Grangier, Marco Tagliasacchi, et al. Audiolum: a
 582 language modeling approach to audio generation. *IEEE/ACM transactions on audio, speech, and
 583 language processing*, 31:2523–2533, 2023.

584 Tom Brown, Benjamin Mann, Nick Ryder, Melanie Subbiah, Jared D Kaplan, Prafulla Dhariwal,
 585 Arvind Neelakantan, Pranav Shyam, Girish Sastry, Amanda Askell, et al. Language models are
 586 few-shot learners. *Advances in neural information processing systems*, 33:1877–1901, 2020.

587
 588 Edresson Casanova, Kelly Davis, Eren Gölge, Görkem Göknar, Iulian Gulea, Logan Hart, Aya Al-
 589 jafari, Joshua Meyer, Reuben Morais, Samuel Olayemi, and Julian Weber. Xtt: a massively
 590 multilingual zero-shot text-to-speech model. *Interspeech*, pp. 4978–4982, 2024.

591
 592 Yunkee Chae, Woosung Choi, Yuhta Takida, Junghyun Koo, Yukara Ikemiya, Zhi Zhong, Kin Wai
 593 Cheuk, Marco A Martínez-Ramírez, Kyogu Lee, Wei-Hsiang Liao, et al. Variable bitrate residual
 vector quantization for audio coding. In *IEEE International Conference on Acoustics, Speech and
 594 Signal Processing*, pp. 1–5, 2025.

594 Ricky TQ Chen, Yulia Rubanova, Jesse Bettencourt, and David K Duvenaud. Neural ordinary
 595 differential equations. *Advances in neural information processing systems*, 31, 2018.
 596

597 Sanyuan Chen, Chengyi Wang, Zhengyang Chen, Yu Wu, Shujie Liu, Zhuo Chen, Jinyu Li, Naoyuki
 598 Kanda, Takuya Yoshioka, Xiong Xiao, et al. Wavlm: Large-scale self-supervised pre-training for
 599 full stack speech processing. *IEEE Journal of Selected Topics in Signal Processing*, 16(6):1505–
 600 1518, 2022.

601 Yushen Chen, Zhikang Niu, Ziyang Ma, Keqi Deng, Chunhui Wang, Jian Zhao, Kai Yu, and Xie
 602 Chen. F5-tts: A fairytaler that fakes fluent and faithful speech with flow matching. *arXiv preprint*
 603 *arXiv:2410.06885*, 2025.

604 Yu-An Chung, Yu Zhang, Wei Han, Chung-Cheng Chiu, James Qin, Ruoming Pang, and Yonghui
 605 Wu. W2v-bert: Combining contrastive learning and masked language modeling for self-
 606 supervised speech pre-training. In *IEEE Automatic Speech Recognition and Understanding Work-
 607 shop*, pp. 244–250, 2021.

608 Alexandre Défossez, Jade Copet, Gabriel Synnaeve, and Yossi Adi. High fidelity neural audio
 609 compression. *arXiv preprint arXiv:2210.13438*, 2022.

610 Alexandre Défossez, Laurent Mazaré, Manu Orsini, Amélie Royer, Patrick Pérez, Hervé Jégou,
 611 Edouard Grave, and Neil Zeghidour. Moshi: a speech-text foundation model for real-time dia-
 612 logue. *arXiv preprint arXiv:2410.00037*, 2024.

613 Jacob Devlin, Ming-Wei Chang, Kenton Lee, and Kristina Toutanova. Bert: Pre-training of deep
 614 bidirectional transformers for language understanding. In *Proceedings of the 2019 conference of
 615 the North American chapter of the association for computational linguistics: human language
 616 technologies*, volume 1, pp. 4171–4186, 2019.

617 Sander Dieleman, Charlie Nash, Jesse Engel, and Karen Simonyan. Variable-rate discrete represen-
 618 tation learning. *arXiv preprint arXiv:2103.06089*, 2021.

619 Zhihao Du, Qian Chen, Shiliang Zhang, Kai Hu, Heng Lu, Yexin Yang, Hangrui Hu, Siqi Zheng, Yue
 620 Gu, Ziyang Ma, et al. Cosyvoice: A scalable multilingual zero-shot text-to-speech synthesizer
 621 based on supervised semantic tokens. *arXiv preprint arXiv:2407.05407*, 2024a.

622 Zhihao Du, Yuxuan Wang, Qian Chen, Xian Shi, Xiang Lv, Tianyu Zhao, Zhifu Gao, Yexin Yang,
 623 Changfeng Gao, Hui Wang, et al. Cosyvoice 2: Scalable streaming speech synthesis with large
 624 language models. *arXiv preprint arXiv:2412.10117*, 2024b.

625 Patrick Esser, Robin Rombach, and Bjorn Ommer. Taming transformers for high-resolution image
 626 synthesis. In *Proceedings of the IEEE/CVF conference on computer vision and pattern recogni-
 627 tion*, pp. 12873–12883, 2021.

628 Qingkai Fang, Shoutao Guo, Yan Zhou, Zhengrui Ma, Shaolei Zhang, and Yang Feng. LLaMA-
 629 omni: Seamless speech interaction with large language models. In *The Thirteenth International
 630 Conference on Learning Representations*, 2025.

631 Aaron Grattafiori, Abhimanyu Dubey, Abhinav Jauhri, Abhinav Pandey, Abhishek Kadian, Ahmad
 632 Al-Dahle, Aiesha Letman, Akhil Mathur, Alan Schelten, Alex Vaughan, et al. The llama 3 herd
 633 of models. *arXiv preprint arXiv:2407.21783*, 2024.

634 Hao-Han Guo, Yao Hu, Fei-Yu Shen, Xu Tang, Yi-Chen Wu, Feng-Long Xie, and Kun Xie.
 635 Fireredtts-1s: An upgraded streamable foundation text-to-speech system. *arXiv preprint*
 636 *arXiv:2503.20499*, 2025a.

637 Yiwei Guo, Zhihan Li, Hankun Wang, Bohan Li, Chongtian Shao, Hanglei Zhang, Chenpeng Du,
 638 Xie Chen, Shujie Liu, and Kai Yu. Recent advances in discrete speech tokens: A review. *arXiv*
 639 *preprint arXiv:2502.06490*, 2025b.

640 Haorui He, Zengqiang Shang, Chaoren Wang, Xuyuan Li, Yicheng Gu, Hua Hua, Liwei Liu, Chen
 641 Yang, Jiaqi Li, Peiyang Shi, et al. Emilia: An extensive, multilingual, and diverse speech dataset
 642 for large-scale speech generation. In *IEEE Spoken Language Technology Workshop*, pp. 885–890,
 643 2024.

648 Tianxing He, Jingzhao Zhang, Zhiming Zhou, and James Glass. Exposure bias versus self-recovery:
 649 Are distortions really incremental for autoregressive text generation? In *Proceedings of the 2021*
 650 *Conference on Empirical Methods in Natural Language Processing*, pp. 5087–5102, 2021.

651 Jonathan Ho and Tim Salimans. Classifier-free diffusion guidance. *arXiv preprint*
 652 *arXiv:2207.12598*, 2022.

653 Wei-Ning Hsu, Benjamin Bolte, Yao-Hung Hubert Tsai, Kushal Lakhotia, Ruslan Salakhutdinov,
 654 and Abdelrahman Mohamed. Hubert: Self-supervised speech representation learning by masked
 655 prediction of hidden units. *IEEE/ACM transactions on audio, speech, and language processing*,
 656 29:3451–3460, 2021.

657 Shengpeng Ji, Ziyue Jiang, Wen Wang, Yifu Chen, Minghui Fang, Jialong Zuo, Qian Yang, Xize
 658 Cheng, Zehan Wang, Ruiqi Li, Ziang Zhang, Xiaoda Yang, Rongjie Huang, Yidi Jiang, Qian
 659 Chen, Siqi Zheng, and Zhou Zhao. Wavtokenizer: an efficient acoustic discrete codec tokenizer
 660 for audio language modeling. In *The Thirteenth International Conference on Learning Representations*, 2025.

661 Daejin Jo, Jeeyoung Yun, Byungseok Roh, and Sungwoong Kim. Lm-spt: Lm-aligned semantic
 662 distillation for speech tokenization. *arXiv preprint arXiv:2506.16738*, 2025.

663 Tero Karras, Miika Aittala, Jaakko Lehtinen, Janne Hellsten, Timo Aila, and Samuli Laine. Analyz-
 664 ing and improving the training dynamics of diffusion models. In *Proceedings of the IEEE/CVF*
 665 *Conference on Computer Vision and Pattern Recognition*, pp. 24174–24184, 2024.

666 W Bastiaan Kleijn, Andrew Storus, Michael Chinen, Tom Denton, Felicia SC Lim, Alejandro Luebs,
 667 Jan Skoglund, and Hengchin Yeh. Generative speech coding with predictive variance regulariza-
 668 tion. In *IEEE International Conference on Acoustics, Speech and Signal Processing*, pp. 6478–
 669 6482, 2021.

670 Rithesh Kumar, Prem Seetharaman, Alejandro Luebs, Ishaan Kumar, and Kundan Kumar. High-
 671 fidelity audio compression with improved rvqgan. *Advances in Neural Information Processing*
 672 *Systems*, 36:27980–27993, 2023.

673 Kushal Lakhotia, Eugene Kharitonov, Wei-Ning Hsu, Yossi Adi, Adam Polyak, Benjamin Bolte,
 674 Tu-Anh Nguyen, Jade Copet, Alexei Baevski, Abdelrahman Mohamed, et al. On generative
 675 spoken language modeling from raw audio. *Transactions of the Association for Computational*
 676 *Linguistics*, 9:1336–1354, 2021.

677 Jiaqi Li, Xiaolong Lin, Zhekai Li, Shixi Huang, Yuancheng Wang, Chaoren Wang, Zhenpeng Zhan,
 678 and Zhizheng Wu. Dualcodec: A low-frame-rate, semantically-enhanced neural audio codec for
 679 speech generation. *arXiv preprint arXiv:2505.13000*, 2025.

680 Yaron Lipman, Ricky TQ Chen, Heli Ben-Hamu, Maximilian Nickel, and Matt Le. Flow matching
 681 for generative modeling. In *11th International Conference on Learning Representations*, 2023.

682 Ilya Loshchilov and Frank Hutter. Decoupled weight decay regularization. *arXiv preprint*
 683 *arXiv:1711.05101*, 2017a.

684 Ilya Loshchilov and Frank Hutter. SGDR: Stochastic gradient descent with warm restarts. In *Inter-
 685 national Conference on Learning Representations*, 2017b.

686 Fabian Mentzer, David Minnen, Eirikur Agustsson, and Michael Tschannen. Finite scalar quantiza-
 687 tion: VQ-VAE made simple. In *The Twelfth International Conference on Learning Representa-
 688 tions*, 2024.

689 OpenAI. Gpt-4 technical report. *arXiv preprint arXiv:2303.08774*, 2024.

690 Julian D Parker, Anton Smirnov, Jordi Pons, CJ Carr, Zack Zukowski, Zach Evans, and Xubo Liu.
 691 Scaling transformers for low-bitrate high-quality speech coding. In *The Thirteenth International*
 692 *Conference on Learning Representations*, 2025.

693 William Peebles and Saining Xie. Scalable diffusion models with transformers. In *Proceedings of*
 694 *the IEEE/CVF international conference on computer vision*, pp. 4195–4205, 2023.

702 Puyuan Peng, Po-Yao Huang, Shang-Wen Li, Abdelrahman Mohamed, and David Harwath. Voice-
 703 craft: Zero-shot speech editing and text-to-speech in the wild. In *Proceedings of the 62nd Annual*
 704 *Meeting of the Association for Computational Linguistics*, pp. 12442–12462, 2024.

705

706 Rafael Rafailov, Archit Sharma, Eric Mitchell, Christopher D Manning, Stefano Ermon, and Chelsea
 707 Finn. Direct preference optimization: Your language model is secretly a reward model. *Advances*
 708 *in neural information processing systems*, 36:53728–53741, 2023.

709

710 Chandan KA Reddy, Vishak Gopal, and Ross Cutler. Dnsmos p. 835: A non-intrusive perceptual
 711 objective speech quality metric to evaluate noise suppressors. In *IEEE international conference*
 712 *on acoustics, speech and signal processing*, pp. 886–890, 2022.

713

714 Oren Rippel, Michael Gelbart, and Ryan Adams. Learning ordered representations with nested
 715 dropout. In *International Conference on Machine Learning*, pp. 1746–1754, 2014.

716

717 Antony W Rix, John G Beerends, Michael P Hollier, and Andries P Hekstra. Perceptual evaluation
 718 of speech quality (pesq)-a new method for speech quality assessment of telephone networks and
 719 codecs. In *IEEE international conference on acoustics, speech, and signal processing*, volume 2,
 pp. 749–752, 2001.

720

721 Paul K Rubenstein, Chulayuth Asawaroengchai, Duc Dung Nguyen, Ankur Bapna, Zalán Borsos,
 Félix de Chaumont Quirky, Peter Chen, Dalia El Badawy, Wei Han, Eugene Kharitonov, et al.
 722 Audiopalm: A large language model that can speak and listen. *arXiv preprint arXiv:2306.12925*,
 723 2023.

724

725 Takaaki Saeki, Detai Xin, Wataru Nakata, Tomoki Koriyama, Shinnosuke Takamichi, and Hiroshi
 726 Saruwatari. Utmos: Utokyo-sarulab system for voicemos challenge 2022. *Interspeech*, 2022.

727

728 Zhihong Shao, Peiyi Wang, Qihao Zhu, Runxin Xu, Junxiao Song, Xiao Bi, Haowei Zhang,
 729 Mingchuan Zhang, YK Li, Yang Wu, et al. Deepseekmath: Pushing the limits of mathematical
 730 reasoning in open language models. *arXiv preprint arXiv:2402.03300*, 2024.

731

732 Feiyu Shen, Yiwei Guo, Chenpeng Du, Xie Chen, and Kai Yu. Acoustic bpe for speech genera-
 733 tion with discrete tokens. In *IEEE International Conference on Acoustics, Speech and Signal*
 Processing, pp. 11746–11750, 2024.

734

735 Maohao Shen, Shun Zhang, Jilong Wu, Zhiping Xiu, Ehab AlBadawy, Yiting Lu, Mike Seltzer,
 736 and Qing He. Get large language models ready to speak: A late-fusion approach for speech
 737 generation. In *IEEE International Conference on Acoustics, Speech and Signal Processing*, pp.
 1–5, 2025.

738

739 Hubert Siuzdak. Vocos: Closing the gap between time-domain and fourier-based neural vocoders
 740 for high-quality audio synthesis. *arXiv preprint arXiv:2306.00814*, 2023.

741

742 Hubert Siuzdak, Florian Grötschla, and Luca A Lanzendörfer. Snac: Multi-scale neural audio codec.
 743 *arXiv preprint arXiv:2410.14411*, 2024.

744

745 Yakun Song, Jiawei Chen, Xiaobin Zhuang, Chenpeng Du, Ziyang Ma, Jian Wu, Jian Cong, Dongya
 746 Jia, Zhuo Chen, Yuping Wang, et al. Magicodec: Simple masked gaussian-injected codec for
 747 high-fidelity reconstruction and generation. *arXiv preprint arXiv:2506.00385*, 2025.

748

749 Cees H Taal, Richard C Hendriks, Richard Heusdens, and Jesper Jensen. A short-time objective in-
 750 telligibility measure for time-frequency weighted noisy speech. In *IEEE international conference*
 751 *on acoustics, speech and signal processing*, pp. 4214–4217, 2010.

752

753 Alexander Tong, Kilian Fatras, Nikolay Malkin, Guillaume Huguet, Yanlei Zhang, Jarrid Rector-
 754 Brooks, Guy Wolf, and Yoshua Bengio. Improving and generalizing flow-based generative models
 755 with minibatch optimal transport. *Transactions on Machine Learning Research*, pp. 1–34, 2024.

756

757 Jean-Marc Valin, Koen Vos, and Timothy Terriberry. Definition of the opus audio codec. *IETF RFC*
 758 6716, 2012.

756 Ashish Vaswani, Noam Shazeer, Niki Parmar, Jakob Uszkoreit, Llion Jones, Aidan N Gomez,
 757 Łukasz Kaiser, and Illia Polosukhin. Attention is all you need. *Advances in neural informa-*
 758 *tion processing systems*, 30, 2017.

759 Stephen D Voran. Why some audio signal short-time fourier transform coefficients have nonuniform
 760 phase distributions. In *IEEE International Conference on Multimedia and Expo*, pp. 1–6, 2024.

762 Chengyi Wang, Sanyuan Chen, Yu Wu, Ziqiang Zhang, Long Zhou, Shujie Liu, Zhuo Chen, Yanqing
 763 Liu, Huaming Wang, Jinyu Li, et al. Neural codec language models are zero-shot text to speech
 764 synthesizers. *arXiv preprint arXiv:2301.02111*, 2023.

765 Hanyu Wang, Saksham Suri, Yixuan Ren, Hao Chen, and Abhinav Shrivastava. LARP: Tokenizing
 766 videos with a learned autoregressive generative prior. In *The Thirteenth International Conference*
 767 *on Learning Representations*, 2025.

768 Sanghyun Woo, Shoubhik Debnath, Ronghang Hu, Xinlei Chen, Zhuang Liu, In So Kweon, and
 769 Saining Xie. Convnext v2: Co-designing and scaling convnets with masked autoencoders. In
 770 *Proceedings of the IEEE/CVF conference on computer vision and pattern recognition*, pp. 16133–
 771 16142, 2023.

773 Dongchao Yang, Songxiang Liu, Haohan Guo, Jiankun Zhao, Yuanyuan Wang, Helin Wang, Zeqian
 774 Ju, Xubo Liu, Xueyuan Chen, Xu Tan, et al. Almtokenizer: A low-bitrate and semantic-rich audio
 775 codec tokenizer for audio language modeling. *arXiv preprint arXiv:2504.10344*, 2025.

776 Zhen Ye, Peiwen Sun, Jiahe Lei, Hongzhan Lin, Xu Tan, Zheqi Dai, Qiuqiang Kong, Jianyi Chen,
 777 Jiahao Pan, Qifeng Liu, et al. Codec does matter: Exploring the semantic shortcoming of codec
 778 for audio language model. In *Proceedings of the AAAI Conference on Artificial Intelligence*,
 779 volume 39, pp. 25697–25705, 2025a.

780 Zhen Ye, Xinfu Zhu, Chi-Min Chan, Xinsheng Wang, Xu Tan, Jiahe Lei, Yi Peng, Haohe Liu, Yizhu
 781 Jin, Zheqi Dai, et al. Llasa: Scaling train-time and inference-time compute for llama-based speech
 782 synthesis. *arXiv preprint arXiv:2502.04128*, 2025b.

784 Jiahui Yu, Xin Li, Jing Yu Koh, Han Zhang, Ruoming Pang, James Qin, Alexander Ku, Yuanzhong
 785 Xu, Jason Baldridge, and Yonghui Wu. Vector-quantized image modeling with improved VQ-
 786 GAN. In *International Conference on Learning Representations*, 2022.

787 Qihang Yu, Mark Weber, Xueqing Deng, Xiaohui Shen, Daniel Cremers, and Liang-Chieh Chen.
 788 An image is worth 32 tokens for reconstruction and generation. *Advances in Neural Information*
 789 *Processing Systems*, 37:128940–128966, 2024.

791 Neil Zeghidour, Alejandro Luebs, Ahmed Omran, Jan Skoglund, and Marco Tagliasacchi. Sound-
 792 stream: An end-to-end neural audio codec. *IEEE/ACM Transactions on Audio, Speech, and*
 793 *Language Processing*, 30:495–507, 2021.

794 Heiga Zen, Viet Dang, Rob Clark, Yu Zhang, Ron J Weiss, Ye Jia, Zhifeng Chen, and Yonghui Wu.
 795 Libritts: A corpus derived from librispeech for text-to-speech. *arXiv preprint arXiv:1904.02882*,
 796 2019.

797 Aohan Zeng, Zhengxiao Du, Mingdao Liu, Lei Zhang, Yuxiao Dong, Jie Tang, et al. Scaling speech-
 798 text pre-training with synthetic interleaved data. In *The Thirteenth International Conference on*
 799 *Learning Representations*, 2025.

801 Dong Zhang, Shimin Li, Xin Zhang, Jun Zhan, Pengyu Wang, Yaqian Zhou, and Xipeng Qiu.
 802 Speechgpt: Empowering large language models with intrinsic cross-modal conversational abil-
 803 ities. In *Findings of the Association for Computational Linguistics: EMNLP 2023*, pp. 15757–
 804 15773, 2023.

805 Hanglei Zhang, Yiwei Guo, Zhihan Li, Xiang Hao, Xie Chen, and Kai Yu. Unlocking temporal
 806 flexibility: Neural speech codec with variable frame rate. *arXiv preprint arXiv:2505.16845*, 2025.

807 Xin Zhang, Dong Zhang, Shimin Li, Yaqian Zhou, and Xipeng Qiu. Speechtokenizer: Unified
 808 speech tokenizer for speech language models. In *The Twelfth International Conference on Learn-
 809 ing Representations*, 2024.

810 A NESTED DROPOUT
811

812 Due to the nature of nested dropout, coarse tokens are more likely to be retained during training,
813 whereas fine tokens are more likely to be dropped, leading to fewer effective gradient updates for
814 the latter. To compensate for this imbalance, we rescale the gradient of each token according to its
815 retention probability p . Specifically, the coarsest token, *i.e.*, the first learnable token in each group,
816 is always retained, while the finest token, *i.e.*, the last learnable token, is retained with probability
817 $1/n_q$, since we uniformly sample the number of tokens to retain. More generally, the retention
818 probability of the j -th token is defined as:

$$819 \quad p_j = 1 - \frac{j-1}{n_q}, \text{ where } j \in [1, n_q]. \quad (14)$$

820 We fix the compensation weight for the first token to 0.5, and accordingly define the weight for each
821 token as:

$$822 \quad w_j = \frac{0.5}{p_j}, \text{ where } j \in [1, n_q]. \quad (15)$$

823 Let the quantized features of the i -th group be $\bar{q}^i \in \mathbb{R}^{n_q \times d_h}$. During the forward pass, we apply the
824 reparameterization trick to scale the token representations as:

$$825 \quad \bar{q}^i[j] \leftarrow \frac{0.5}{p_j} \bar{q}^i[j] + \left(\bar{q}^i[j] - \frac{0.5}{p_j} \bar{q}^i[j] \right) .\text{detach}, \quad (16)$$

826 where $\bar{q}^i[j]$ denotes the j -th token in group i , and the `detach` operator indicates that the gradient flow
827 is stopped for the detached variable. By applying Equation 16, the value of each embedding $\bar{q}^i[j]$
828 remains unchanged during the forward pass. However, in the backward pass, its gradient is scaled by
829 the inverse of p_j to offset the imbalance in p_j . As a result, $\bar{q}^i[j]$ that receive fewer gradient updates
830 are compensated with a larger gradient scale.

831 B AUXILIARY MODULES
832

833 The AR prior takes the quantized representations \bar{q}^i as input and predicts the feature representation
834 of the next speech token at every position. To enhance training stability, the AR prior is optimized
835 with a mean squared error loss in the feature space. Let f denotes the AR prior with parameters η .
836 The AR loss is defined as:

$$837 \quad \mathcal{L}_{\text{AR}} = \mathbb{E}_i \left[\frac{1}{n_q - 1} \sum_{j=1}^{n_q-1} \left\| f_\eta \left(\bar{q}^i[1:j] \right) - \bar{q}^i[j+1] \right\|_2^2 \right]. \quad (17)$$

840 Furthermore, we incorporate an ASR module into the Gogo training pipeline to facilitate the linguistic
841 representation learning. The group-wise quantized representations $\bar{q}^i \in \mathbb{R}^{n_q \times d_h}$ are concatenated
842 along the temporal dimension to form $\bar{x}_s \in \mathbb{R}^{n_q(n_f/g) \times d_h}$. The ASR module, denoted as h_ϕ , takes
843 \bar{x}_s as input and outputs a predicted token sequence $\hat{y} = (\hat{y}_1, \dots, \hat{y}_L)$ corresponding to the ground-
844 truth transcription $y = (y_1, \dots, y_L)$. The ASR loss is formulated as the cross entropy loss:

$$845 \quad \mathcal{L}_{\text{ASR}} = \mathbb{E}_{(\bar{x}_s, y)} \left[-\frac{1}{L} \sum_{t=1}^L \log h_\phi(y_t | y_{<t}, \bar{x}_s) \right]. \quad (18)$$

846 C MODEL CONFIGURATION DETAILS
847

848 For Gogo, the Transformer encoder, ASR module, and AR prior are implemented with 12, 8, and 4
849 layers of standard Transformer blocks (Vaswani et al., 2017), respectively, following the architecture
850 of LLaMA (Grattafiori et al., 2024). Each layer uses a hidden dimension of 512, 8 attention heads,
851 a feed-forward dimension of 1536, Rotary Position Embeddings (RoPE), RMSNorm, and SwiGLU
852 activation. **Asymmetric masking is applied in the Transformer encoder such that mel features can**
853 **attend to each other but not to the speech queries, whereas each speech query has access to all**
854 **mel features and to its preceding queries.** We set the group size to $g = 20$, and allocate $n_q = 10$

864 speech queries per group. The feature quantization adopts FSQ with levels [8, 8, 8, 5, 5], yielding
 865 an effective codebook size of 12,800. The flow-matching model in Gogo is implemented as a latent
 866 Diffusion Transformer (DiT) (Peebles & Xie, 2023), following the configuration of Chen et al.
 867 (2025). The only modification is that we set the number of layers to 12. Additionally, the input mel-
 868 spectrograms of Gogo are first processed by four ConvNeXt V2 (Woo et al., 2023) layers, followed
 869 by a two-layer MLP that projects the features to match the hidden dimension of Gogo.

870 For GogoSpeech, both Stage I and Stage II are built on top of Llama-3.2-1B-Instruct, with the
 871 vocabulary extended to include Gogo’s codebook tokens, enabling the model to directly perform
 872 speech token generation. GogoSpeech is trained under the next-token prediction paradigm to jointly
 873 model text and speech tokens. The maximum sequence length is set to 256 and 1024 tokens for
 874 Stage I and Stage II, respectively. The speech backbone is defined as the first $b = 3$ tokens of each
 875 group, which are generated in Stage I. The remaining 7 tokens per group are recovered in Stage II.

876 For the token allocator, we adopt a lightweight Transformer with 2 layers and the same architectural
 877 configuration used in Gogo, followed by a linear classifier to predict the token budget for each group.
 878

880 D TRAINING AND INFERENCE DETAILS

882 Gogo, GogoSpeech, and the token allocator are optimized separately using the AdamW optimizer
 883 (Loshchilov & Hutter, 2017a) on 8 NVIDIA H100 NVL 94G GPUs. The learning rate is decayed
 884 based on a cosine annealing schedule (Loshchilov & Hutter, 2017b). Speech samples longer than
 885 20 seconds or shorter than 1 seconds are discarded during training. More detailed training hyperpa-
 886 rameters are shown in Table 4.

887
 888 Table 4: Hyperparameters for training Gogo, GogoSpeech, and the token allocator.
 889

890 Hyperparameters	891 Gogo	892 GogoSpeech Stage I / Stage II	893 Token Allocator
894 Training Epochs	895 -	896 10 / 5	897 1
898 Update Steps	900 400k	901 -	902 -
903 Warmup Steps	905 10k	906 5k / 10k	907 1k
908 Batch Size	910 1440 Seconds	911 1152 / 288 Samples	912 128 Samples
913 Learning Rate	915 2e-4	916 5e-4	917 1e-4
918 Optimizer	920 AdamW	921 AdamW	922 AdamW
923 Momentum	925 $\beta_1, \beta_2 = 0.9, 0.999$	926 $\beta_1, \beta_2 = 0.9, 0.95$	927 $\beta_1, \beta_2 = 0.9, 0.999$
928 Weight Decay	930 0.01	931 0.01	932 0.01
933 Learning Rate Schedule	935 Cosine Annealing	936 Cosine Annealing	937 Cosine Annealing

901
 902 For Gogo inference, we begin from sampled Gaussian noise x_0 and integrate it toward the target
 903 distribution x_1 conditioned on the speech tokens s^i . Following Eq. 1 and Eq. 2, the tokens s^i are first
 904 converted into aligned representations \bar{x} . We then employ an Euler ordinary differential equation
 905 (ODE) solver to iteratively integrate $\partial x_t / \partial t = v_\theta(x_t, \bar{x}, t)$ from x_0 to x_1 , where the flow step t is
 906 sampled using the Sway Sampling strategy (Chen et al., 2025) to improve generation performance
 907 and efficiency. The resulting mel-spectrogram x_1 is converted into waveform using a pretrained
 908 Vocos vocoder (Siuzdak, 2023). To balance fidelity and diversity, we apply Classifier-Free Guidance
 909 (CFG) (Ho & Salimans, 2022) with a guidance scale of 2. For further stability, Exponential Moving
 910 Averaged (EMA) weights (Karras et al., 2024) of the model parameters are used during inference.

911 For GogoSpeech inference, we employ the standard autoregressive decoding strategy widely used
 912 in large language models. To balance generation diversity and fidelity, we set the temperature to
 913 0.8, apply a repetition penalty of 1.2 to mitigate degenerate loops, and use nucleus sampling with
 914 $p = 1.0$. In Stage II of GogoSpeech, decoding for each group employs early stopping, terminating
 915 as soon as the maximum token budget assigned by the token allocator is consumed.

916 For token allocator inference, the first b tokens of each group (three tokens in our case) produced
 917 by Stage I of GogoSpeech are used as input. The allocator then predicts a budget for the group,
 specifying how many fine tokens should be generated in Stage II.

918 E CODEC BASELINES
919920 **EnCodec** (Défossez et al., 2022) builds upon the residual vector quantization (RVQ) framework and
921 employs a single multi-scale STFT-based discriminator to effectively suppress artifacts and enhance
922 perceptual quality. It supports variable bandwidths by selecting different numbers of codebooks
923 during training, providing a flexible solution for speech compression and discretization in speech
924 language models. For evaluation, we adopt the official implementation and pretrained checkpoint¹.925 **DAC** (Kumar et al., 2023) adapts advances from the Improved VQGAN (Yu et al., 2022) image
926 model to address the codebook collapse problem. It performs codebook lookup in a low-dimensional
927 space and replaces Euclidean distance with cosine similarity, improving both stability and quality.
928 DAC further employs a multi-period discriminator in the waveform domain and a multi-band, multi-
929 scale STFT discriminator in the frequency domain, enabling high-fidelity audio generation. For
930 evaluation, we use the official implementation and pretrained checkpoint².931 **SpeechTokenizer** (Zhang et al., 2024) is specifically designed for speech language modeling, where
932 different aspects of speech are disentangled hierarchically across RVQ layers. Specifically, it em-
933 ploys HuBERT as a semantic teacher to distill content information into the first layer of RVQ. For
934 evaluation, we use the official implementation and pretrained checkpoint³.935 **Mimi** (Défossez et al., 2024) takes inspiration from previous work on SpeechTokenizer and uses
936 distillation to transfer high-level semantic information in WavLM into the quantized tokens. Unlike
937 SpeechTokenizer, it distills semantic information into a plain VQ and apply an RVQ with 7 levels in
938 parallel, thereby removing the constraint that acoustic information must reside in the residual of the
939 semantic quantizer. For evaluation, we use the official implementation and pretrained checkpoint⁴.940 **SNAC** (Siuzdak et al., 2024) extends RVQ by allowing quantizers to operate at different temporal
941 resolutions. Through a hierarchy of quantizers running at variable frame rates, it adapts to audio
942 structure across multiple timescales, thereby capturing both coarse and fine details more effectively.
943 Each quantizer applies average pooling for downsampling and nearest-neighbor interpolation for
944 upsampling, enabling efficient compression. For evaluation, we adopt the official implementation
945 and pretrained checkpoint⁵.946 **WavTokenizer** (Ji et al., 2025) improves subjective quality using a single quantizer with an ex-
947 panded codebook to reduce information loss. It further enhances semantic modeling by introducing
948 attention modules with extended contextual windows in the decoder. Finally, the inverse Fourier
949 transform is employed to reconstruct the final audio directly. For evaluation, we adopt the official
950 implementation and pretrained checkpoint⁶.951 **MagiCodec** (Song et al., 2025) is a single-layer, streaming Transformer-based audio codec trained
952 with a multistage pipeline to mitigate codebook collapse and improve token efficiency. It introduces
953 Gaussian noise injection and latent regularization techniques to encourage learning low-frequency
954 semantic representations while preventing overfitting to high-frequency noise. For evaluation, we
955 adopt the official implementation and pretrained checkpoint⁷.956 **X-codec2** (Ye et al., 2025b) integrates semantic and acoustic features into a unified codebook using
957 a single-layer FSQ quantizer. A pretrained w2v-BERT serves as the semantic encoder, while an
958 acoustic encoder based on residual convolutional blocks with Snake activations captures fine-grained
959 acoustic details. The semantic and acoustic features are concatenated and served as input to the
960 vector quantizer. For evaluation, we adopt the official implementation and pretrained checkpoint⁸.961 **TAAE** (Parker et al., 2025) introduces a Transformer-based codec architecture that scales into the
962 1B parameter range, enabling state-of-the-art speech quality at extremely low bitrates. Unlike CNN-
963 based codecs that rely on convolutional inductive biases with high parameter efficiency, TAAE lever-964 ¹<https://github.com/facebookresearch/encodec>965 ²<https://github.com/descriptinc/descript-audio-codec>966 ³<https://github.com/ZhangXInFD/SpeechTokenizer>967 ⁴<https://huggingface.co/kyutai/mimi>968 ⁵<https://github.com/hubertsiuzdak/snac>969 ⁶<https://github.com/jishengpeng/WavTokenizer>970 ⁷<https://github.com/Ereboas/MagiCodec>971 ⁸<https://huggingface.co/HKUSTAudio/xcodec2>

ages a more general Transformer architecture for greater scalability and better modeling capacity. For evaluation, we adopt the official implementation and pretrained checkpoint⁹.

DualCodec (Li et al., 2025) is a dual-stream codec that jointly models self-supervised and waveform representations within an end-to-end framework. The first RVQ layer directly encodes semantic-rich features from a pretrained w2v-BERT-2 model, while the remaining RVQ layers, along with the encoder–decoder design, follow the DAC framework. This integration enables DualCodec to better preserve linguistic content while maintaining high-fidelity reconstruction. For evaluation, we use the official implementation and pretrained checkpoint¹⁰.

F TTS BASELINES

FireRedTTS-1S (Guo et al., 2025a) is a high-quality streamable TTS system that achieves real-time speech generation with low latency under 150ms through text-to-semantic decoding and semantic-to-acoustic decoding. For evaluation, we use the pretrained checkpoint¹¹.

F5-TTS Chen et al. (2025) is a non-autoregressive TTS model built on flow matching. Instead of relying on complex alignment mechanisms, F5-TTS pads the text input with filler tokens to match the length of the target speech and directly performs denoising to generate speech. For evaluation, we use the pretrained checkpoint¹².

XTTS-v2 (Casanova et al., 2024) is a multilingual zero-shot multi-speaker TTS model built upon the Tortoise model (Betker, 2023). XTTS-v2 supports 16 languages and achieves state-of-the-art results in most of them. For evaluation, we use the pretrained checkpoint¹³.

Llasa (Ye et al., 2025b) is a large-scale speech synthesis system that employs a single-layer vector quantizer codec and a unified Transformer architecture to fully align with standard LLMs such as Llama. For evaluation, we use the pretrained checkpoint¹⁴.

CosyVoice 2 (Du et al., 2024b) is a multilingual speech synthesis framework that integrates a pre-trained language model for discrete speech token prediction with a chunk-aware flow-matching model for speech feature generation. For evaluation, we use the pretrained checkpoint¹⁵.

VoiceCraft (Peng et al., 2024) is a token infilling neural codec language mode. It employs a token rearrangement strategy with causal masking and delayed stacking, enabling seamless speech editing and zero-shot text-to-speech generation. For evaluation, we use the pretrained checkpoint¹⁶.

G EVALUATION METRICS

We employ a comprehensive set of evaluation metrics to assess speech quality across multiple dimensions, including intelligibility, perceptual quality, content preservation, and speaker similarity.

Short-Time Objective Intelligibility (STOI) (Taal et al., 2010) is a widely adopted metric for evaluating speech intelligibility. It computes the correlation between temporal envelopes of reference and reconstructed signals in short-time segments. The score ranges from 0 to 1, with higher values indicating better intelligibility.

Perceptual Evaluation of Speech Quality (PESQ) (Rix et al., 2001) measures perceptual speech quality by comparing the reconstructed audio with the clean reference signal using a perceptual auditory model. We report results under both narrow-band (NB, 8 kHz) and wide-band (WB, 16 kHz) conditions.

⁹<https://github.com/Stability-AI/stable-codec>

¹⁰<https://github.com/jiaqili3/DualCodec>

¹¹<https://github.com/FireRedTeam/FireRedTTS>

¹²<https://github.com/SWivid/F5-TTS>

¹³<https://huggingface.co/coqui/XTTS-v2>

¹⁴<https://huggingface.co/HKUSTAudio/Llasa-8B>

¹⁵<https://huggingface.co/FunAudioLIM/CosyVoice2-0.5B>

¹⁶https://huggingface.co/pyp1/VoiceCraft/blob/main/830M_TTSEnhanced.pth

1026 **UTokyo-SaruLab MOS (UT-MOS)** (Saeki et al., 2022) is an automatic MOS predictor trained
 1027 to approximate human judgments of overall speech naturalness and quality. It provides a scalable
 1028 alternative to subjective MOS tests.

1029 **Deep Noise Suppression MOS (DNS-MOS)** (Reddy et al., 2022) is a non-intrusive quality metric
 1030 designed for real-world audio evaluation. It estimates perceptual quality directly from the signal
 1031 without requiring reference audio and has been shown to correlate strongly with human ratings.

1032 **Word Error Rate (WER)** is used to quantify content preservation and intelligibility at the linguistic
 1033 level. By default, we adopt HuBERT as the ASR model¹⁷ to transcribe the reconstructed speech,
 1034 and compute WER by comparing against the ground-truth transcripts. For zero-shot TTS evaluation
 1035 on the Seed-TTS test-en set, the WER metric is computed using the provided script¹⁸.

1036 **Speaker Similarity (SIM)** measures the degree to which the synthesized speech retains the identity
 1037 of the original speaker. By default, we follow Wang et al. (2023) and employ a WavLM-Large-based
 1038 speaker verification model¹⁹ to extract speaker embeddings from both reconstructed and reference
 1039 speech, and compute cosine similarity as the final metric. For zero-shot TTS evaluation on the
 1040 Seed-TTS test-en set, the SIM metric is computed using the provided script¹⁸.

1041 **Similarity Mean Opinion Score (SMOS)** evaluates the speaker similarity between the prompt and
 1042 the generated speech. Human raters judge the degree of resemblance by considering speaker char-
 1043 acteristics, style, acoustic properties, and potential background artifacts. SMOS is scored on a
 1044 five-point scale, with higher values indicating stronger similarity.

1045 **Comparative Mean Opinion Score (CMOS)** measures the relative perceptual quality of a synthe-
 1046 sized sample compared to a reference. Raters assign scores on a scale from -3 to 3, where negative
 1047 values indicate the synthesized speech is worse than the reference, positive values indicate it is better,
 1048 and 0 denotes parity.

1049 **For subjective evaluation, we randomly select 20 samples from the Seed-TTS test-en set and invite
 1050 20 listeners to rate the SMOS and CMOS scores for the synthesized samples.**

1053 H PROBING EXPERIMENTS

1054 The probing model consists of three fully connected layers with ReLU activations and dropout in
 1055 between. The hidden dimensions of each layer are 512, 128, and 1, respectively. The probing
 1056 procedure is formulated as a regression task. **Given a speech input, we first extract the target feature
 1057 to be probed. Next, Gogo is used to quantize the speech and generate multiple groups of tokens. To
 1058 probe the tokens at position 8, as illustrated in Figure 6, we average the tokens at this position across
 1059 all groups. The resulting averaged representation is then fed into the probing model to predict the
 1060 value of the target feature.** The mean squared error (MSE) loss of the probing model is reported as
 1061 an indicator of the representational capacity of tokens at each position, with lower loss implying that
 1062 the token more readily encodes the probed feature.

1063 We conduct probing experiments on Gogo’s granularity-ordered tokens using a broad set of features
 1064 spanning acoustic, prosodic, and linguistic dimensions. Acoustic features include zero-crossing
 1065 rate, mean pitch, energy entropy, and spectral centroid, which characterize low-level signal proper-
 1066 ties. Prosodic features include jitter, shimmer, duration, voiced–unvoiced ratio, and speaking rate,
 1067 capturing rhythm, intonation, and phonation stability. Linguistic features include lexical statistics
 1068 such as unique word count and counts of adjectives, adverbs, nouns, verbs, pronouns, and conjunc-
 1069 tions, reflecting higher-level syntactic content. The probing models are trained on the LibriTTS
 1070 train-clean-100 subset for 20k steps using the AdamW optimizer and evaluated on the LibriTTS
 1071 test-clean set. The detailed MSE losses for each feature are reported in Table 5.

1072 We further investigate how reconstruction quality varies when only a subset of the granularity-
 1073 ordered tokens is used. Specifically, we progressively retain the first n tokens in each group and
 1074 reconstruct the input speech, where $n \in [1, n_q]$. The results are shown in Figure 7. We observe
 1075

1076 ¹⁷<https://huggingface.co/facebook/hubert-large-ls960-ft>

1077 ¹⁸<https://github.com/BytedanceSpeech/seed-tts-eval>

1078 ¹⁹https://github.com/microsoft/UniSpeech/tree/main/downstreams/speaker_verification

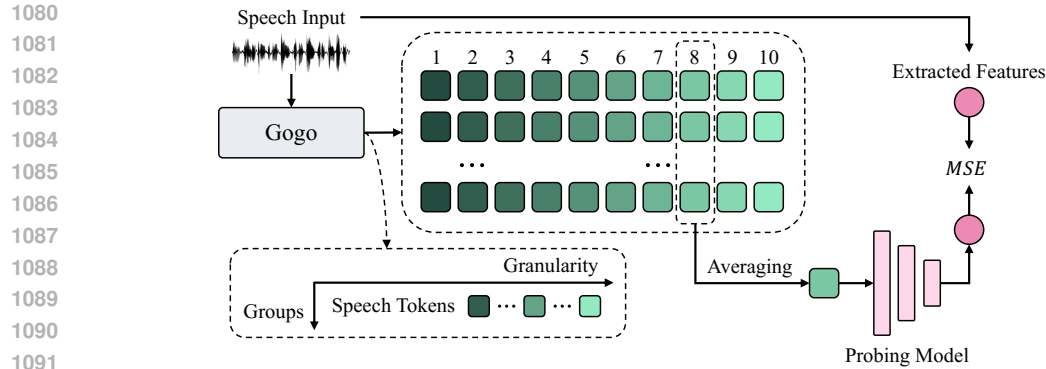


Figure 6: Procedure for probing the information encoded in tokens of different granularities. Throughout the probing model training, the Gogo codec is kept frozen. Here we probe the tokens at position 8 for demonstration.

Table 5: MSE losses for various probed features using Gogo’s granularity-ordered tokens on the LibriTTS test-clean set. In our setting, each frame group is discretized into 10 tokens. Token position 1 corresponds to the coarsest token, whereas position 10 corresponds to the finest; ZRC: zero crossing rate, EE: energy entropy, SC: spectral centroid, J: jitter, S: Shimmer, Ratio: voiced to unvoiced ratio, SR: speaking rate, Count: unique word count, Tadj: total adjectives, Tadv: total adverbs, Tn: total nouns, Tv: total verbs, Tpron: total pronouns, Tconj: total conjunction.

Features	1	2	3	4	5	6	7	8	9	10
Duration	14.44	14.95	15.87	16.28	16.81	16.45	16.59	16.65	17.23	17.45
ZRC (e-3)	1.113	1.058	1.051	1.060	1.076	1.071	1.101	1.047	1.036	1.038
EE (e-3)	8.409	8.290	8.189	8.257	8.142	8.212	8.101	8.066	7.839	7.771
SC (e-3)	1.150	1.053	1.054	1.031	0.988	0.879	0.866	0.830	0.872	0.933
Pitch	1455	1478	1424	1371	1304	1295	1230	1166	1074	1012
J (e-5)	4.000	3.969	3.696	3.603	3.415	3.584	3.445	3.887	3.751	3.563
S (e-4)	3.463	3.497	3.435	3.382	3.321	3.345	3.290	3.377	3.350	3.312
Ratio	0.298	0.297	0.313	0.318	0.332	0.319	0.332	0.323	0.338	0.343
SR	0.414	0.415	0.413	0.406	0.403	0.406	0.411	0.411	0.409	0.409
Count	35.81	36.90	39.01	40.00	41.18	40.34	40.63	40.70	41.96	42.47
Tense	0.240	0.239	0.238	0.237	0.236	0.237	0.237	0.239	0.239	0.238
Tadj	2.229	2.250	2.299	2.329	2.352	2.334	2.337	2.338	2.359	2.370
Tadv	1.474	1.486	1.507	1.521	1.532	1.523	1.521	1.526	1.537	1.538
Tn	9.716	9.907	10.32	10.55	10.81	10.67	10.71	10.66	10.88	10.99
Tv	4.708	4.804	4.969	5.023	5.128	5.057	5.097	5.116	5.240	5.282
Tpron	2.766	2.797	2.838	2.847	2.868	2.847	2.853	2.866	2.897	2.906
Tconj	0.967	0.977	0.998	1.005	1.015	1.003	1.006	1.010	1.024	1.027

that the word error rate drops sharply when the first few tokens are included, indicating that most linguistic content is captured by the coarsest tokens in Gogo. However, when more than six tokens per group are retained, the improvement of WER becomes marginal, suggesting that the remaining fine-grained tokens primarily contribute to perceptual quality and acoustic details rather than linguistic content. In particular, both NB PESQ and WB PESQ scores show a marked improvement once more than four tokens per group are retained. The other objective metrics exhibit a generally monotonic improvement as the number of retained tokens increases.

I PERPLEXITY EXPERIMENTS

Perplexity (PPL) is a standard evaluation metric for language models that quantifies their uncertainty in predicting the next token in a sequence. Lower PPL indicates higher model confidence and

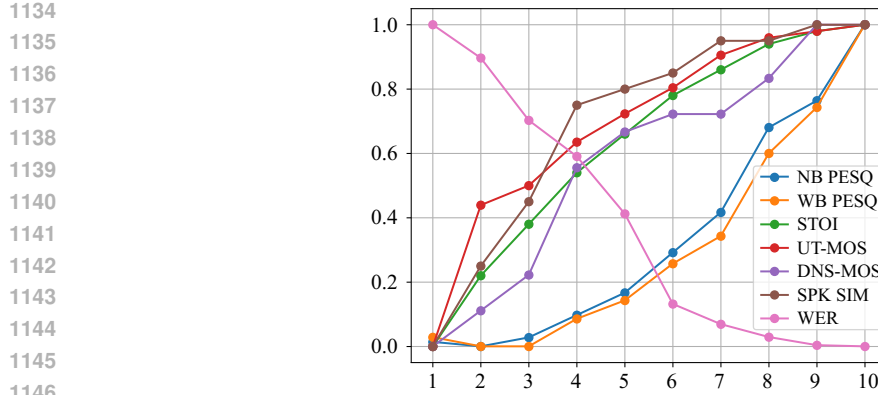


Figure 7: Normalized performance on the LibriTTS test-clean set with varying numbers of retained tokens per group.

prediction accuracy, whereas higher PPL reflects greater uncertainty and poorer predictive performance. Formally, perplexity is defined as the exponentiated average negative log-likelihood of the sequence. In our setting, given a speech token sequence $\Gamma(\mathbf{S}_{:,j})$, where $\mathbf{S} \in \mathbb{R}^{n_g \times n_q}$ is the token matrix produced by Gogo and $j \in [1, n_q]$ denotes the position of the speech token within each group, we compute PPL to assess the autoregressive modeling difficulty at different token granularities as follow:

$$\text{PPL}(\Gamma(\mathbf{S}_{:,j})) = \exp \left\{ -\frac{1}{n_g} \sum_i^{n_g} \log P(\mathbf{S}_{i,j} | \mathbf{S}_{<i,j}) \right\}. \quad (19)$$

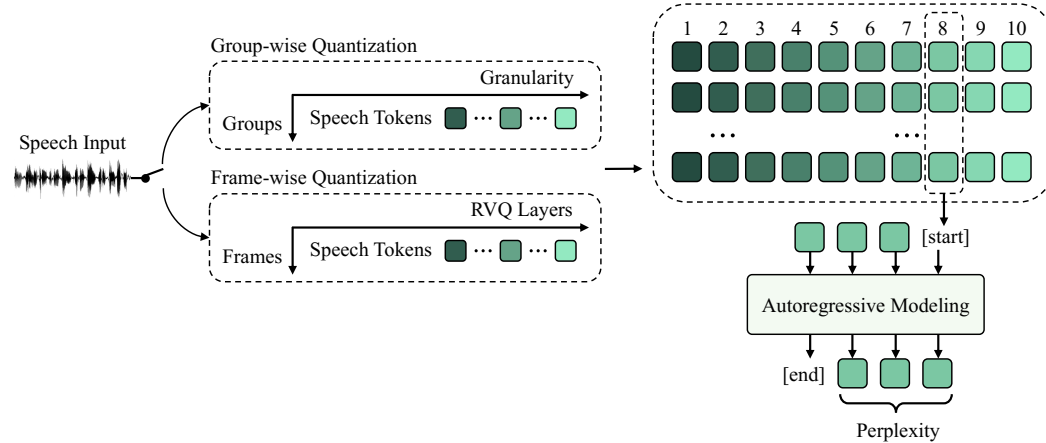


Figure 8: Procedure for evaluating the perplexity of autoregressive model on speech tokens generated by different quantization schemes. Here we show the evaluation using the 8th token of each group or tokens from the 8th RVQ layer for demonstration.

As illustrated in Figure 8, the autoregressive model used in the perplexity experiments is a 6-layer LLaMA-style Transformer with hidden dimension of 256. It is trained on the combined LibriTTS train-clean-100, train-clean-360, and train-other-500 subsets for 200k steps using the AdamW optimizer. Evaluation is conducted on the LibriTTS test-clean set.

J STATISTICAL SIGNIFICANCE ANALYSIS

In Table 6, we report the 95% confidence intervals for all subjective evaluation metrics to characterize score variability across listeners. For CMOS, in which listeners provide paired comparative

judgments, we evaluate statistical significance using the Wilcoxon signed-rank test and include the corresponding p-values. Across models, several systems display statistically significant differences from the Ground Truth, as indicated by p-values ≤ 0.05 . Our proposed GogoSpeech also achieves a statistically significant positive CMOS relative to the Ground Truth, and incorporating the token allocator leads to a similarly significant improvement.

Table 6: Subjective comparison between different TTS models on the Seed-TTS test-en set. The boldface denotes the best result, the underline denotes the second best. We report 95% confidence intervals for all scores and assess statistical significance (p-value) using the Wilcoxon signed-rank test for CMOS. p-value ≤ 0.05 indicate statistical significance.

Model	SMOS	CMOS (p-value)
Ground Truth	4.752 ± 0.342	0.000
F5-TTS (Chen et al., 2025)	4.173 ± 0.513	$+1.730 \pm 0.476 (4.9e-4)$
XTTS-v2 (Casanova et al., 2024)	2.426 ± 0.572	$-0.961 \pm 1.088 (0.072)$
Llasa-8B-250k (Ye et al., 2025b)	3.297 ± 0.533	$+0.882 \pm 0.869 (0.027)$
CosyVoice 2 (Du et al., 2024b)	4.331 ± 0.435	$+1.638 \pm 0.596 (2.9e-3)$
FireRedTTS-1S (Guo et al., 2025a)	4.247 ± 0.409	$+1.634 \pm 0.561 (3.0e-3)$
VoiceCraft (Peng et al., 2024)	2.965 ± 0.697	$-0.751 \pm 0.877 (0.170)$
GogoSpeech (47 Hz)	4.381 ± 0.479	$+1.832 \pm 0.491 (2.7e-3)$
w/ Token Allocator (47 Hz \rightarrow 36 Hz)	4.253 ± 0.344	$+1.587 \pm 0.530 (0.013)$

K ABLATION EXPERIMENTS

Table 7: Ablation study on the auxiliary modules and granularity ordering. Gogo is evaluated on the LibriTTS test-clean set. GogoSpeech is evaluated on the Seed-TTS test-en set.

Model	Gogo							GogoSpeech	
	UT MOS	DNS MOS	STOI	PESQ WB	PESQ NB	SIM	WER	SIM	WER
Auxiliary Module									
Proposed Model	4.19	3.99	0.92	2.59	3.26	0.91	6.35	0.667	2.394
w/o ASR Module	3.97	3.91	0.87	2.63	3.29	0.92	8.66	0.640	4.372
w/o AR Prior	4.14	3.96	0.86	2.61	3.24	0.91	6.42	0.661	2.625
Granularity Ordering									
Proposed Model	4.19	3.99	0.92	2.59	3.26	0.91	6.35	0.667	2.394
w/o Nested Dropout	4.10	3.89	0.89	2.39	3.16	0.89	6.41	0.657	3.969
w/o Loss Balancer	3.89	3.74	0.82	2.29	3.07	0.85	7.50	0.614	4.608

Gogo. We perform an ablation study on all auxiliary modules and design choices in Gogo and further evaluate their impact on GogoSpeech. The results are summarized in Table 7. We can see that removing the ASR module leads to a slight improvement in PESQ and SIM for Gogo’s reconstruction. However, the absence of ASR guidance significantly degrades the performance of GogoSpeech across all metrics. Eliminating the AR prior has little effect on Gogo’s reconstruction metrics but results in a noticeable performance drop for GogoSpeech. This suggests that the AR prior primarily benefits the autoregressive modeling of GogoSpeech rather than signal reconstruction. Furthermore, we ablate the granularity ordering mechanism. We can observe that removing either nested dropout or the loss balancer causes a substantial decline in performance for both Gogo and GogoSpeech, highlighting their importance in learning informative coarse-to-fine token representations.

GogoSpeech. We further perform an ablation study on the number of coarse tokens b used as the speech backbone, with results summarized in Table 8. We observe that increasing b from 1 to 3 yields substantial improvements in both SIM and WER, indicating that a slightly richer backbone provides more effective guidance for Stage II refinement. When b lies between 3 and 5, the performance of both metrics becomes relatively stable, with SIM reaching its peak at $b = 3$ and WER achieving

1242

1243 Table 8: Ablation study on the number of coarse tokens b used as the speech backbone on the
1244 Seed-TTS test-en set. Using all 10 tokens as the backbone degenerates into a single-stage model.

b	1	2	3	4	5	6	7	8	9	10
SIM	0.647	0.654	0.667	0.663	0.662	0.652	0.657	0.656	0.654	0.642
WER	2.754	2.531	2.394	2.391	2.397	2.441	2.346	2.451	2.460	3.121

1245

1246

1247 its best value at $b = 4$. As b increases further from 6 to 9, all evaluation metrics exhibit a general
1248 downward trend, suggesting that overly detailed backbones may limit the capacity of Stage II to
1249 contribute fine-grained refinements. When $b = 10$, meaning that all tokens are generated entirely
1250 within Stage I of GogoSpeech, the performance drops to its lowest level across all metrics. These
1251 results provide strong empirical evidence for the effectiveness of our two-stage design, where a
1252 compact backbone combined with detail refinement yields the best overall performance.
1253

1254

1255

1256 Table 9: Ablation study on the token allocator on the Seed-TTS test-en set. Various token allocators,
1257 trained under different experimental settings, are applied to the same GogoSpeech model.

Model	GogoSpeech	
	SIM	WER
GRPO Modifications		
Proposed Model	0.662	2.469
w/o Removal of KL Penalty	0.647	3.452
w/o Exhaustive Enumeration	0.651	2.659
Sensitivity to Reward Weights		
Proposed Model ($\lambda_n = 0.2, \lambda_d = 1.0$)	0.662	2.469
$\lambda_n = 0.5, \lambda_d = 1.0$	0.656	2.882
$\lambda_n = 1.0, \lambda_d = 1.0$	0.650	3.169
$\lambda_n = 1.0, \lambda_d = 0.5$	0.642	3.772
$\lambda_n = 1.0, \lambda_d = 0.2$	0.643	3.528
Reinforcement Learning Objectives		
Proposed Model	0.662	2.469
Replace GRPO with DPO (Rafailov et al., 2023)	0.645	3.691

1274

1275 **Token Allocator.** We further conduct an ablation study to evaluate the effectiveness of our
1276 modifications to the standard GRPO algorithm, including the removal of the KL penalty and the use
1277 of exhaustive enumeration. We also examine the sensitivity of the token allocator to different re-
1278 ward weights and compare the GRPO-based allocator with its DPO-based counterpart. The results
1279 are summarized in Table 9. We observe that removing the KL penalty and introducing exhaustive
1280 enumeration during allocator training consistently yield performance gains. Moreover, the reward-
1281 sensitivity analysis suggests that greater emphasis should be placed on the reward term \mathcal{R}_d , while
1282 \mathcal{R}_n should be assigned a smaller weight. Finally, the last row of Table 9 shows that the GRPO-based
1283 token allocator outperforms the DPO-based approach.

1284

1285

1286 Table 10: Systematic evaluation of codec and SLM design choices on the Seed-TTS test-en set. The
1287 boldface denotes the best result, the underline denotes the second best.

Codec	SLM		Token Allocator	TPS	SIM	WER
	Frame-wise	Group-wise				
✓		✓		47	0.592	4.117
	✓	✓		47	0.642	3.121
✓			✓	47	0.667	2.394
✓			✓	36	0.662	2.469

1293

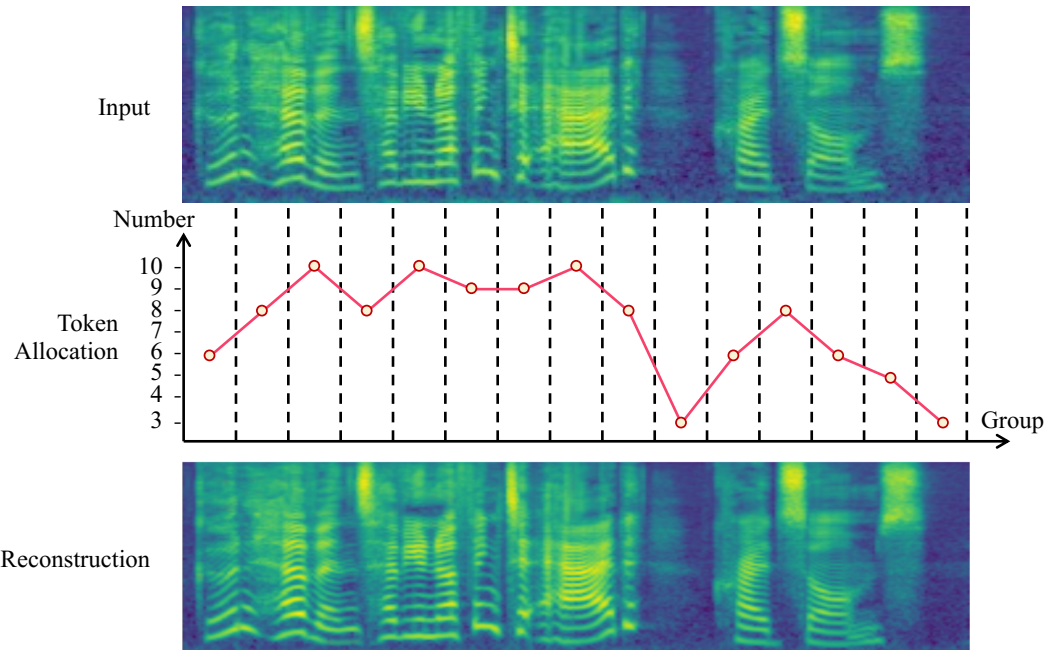
1294

1295 **Systematic Evaluations under Consistent Training Conditions** To rigorously isolate the impact
of our proposed approach and further demonstrate the effectiveness of Gogo, GogoSpeech, and

1296 the token allocator, we conduct a carefully controlled ablation study. The results are reported in
 1297 Table 10. All experiments in the table, including codec and SLM model training, are conducted
 1298 on the Emilia dataset. The frame-wise and group-wise codecs operate at the same token rate, and
 1299 all SLM models are initialized with Llama-3.2-1B-Instruct. Comparing the first and second rows,
 1300 both using a single-stage SLM, we observe that the SLM using the group-wise codec (*i.e.*, Gogo)
 1301 outperforms the one using the frame-wise codec, demonstrating the effectiveness of our group-wise
 1302 quantization. Comparing the second and third rows, both using the group-wise codec, the two-stage
 1303 SLM (*i.e.*, GogoSpeech) achieves higher performance metrics than the single-stage SLM, validating
 1304 the effectiveness of our two-stage design. Finally, comparing the last two rows, the introduction of
 1305 the token allocator reduces the token rate from 47 Hz to 36 Hz while maintaining roughly the same
 1306 model performance, indicating the effectiveness of the token allocator.
 1307

L VISUALIZATION OF TOKEN ALLOCATION

1310 To better illustrate the behavior of the token allocator, we visualize the token allocation results in
 1311 Figure 9 and Figure 10. Specifically, we present three aligned plots: (1) the original mel-spectrogram
 1312 of the input speech, where vertical dashed lines indicate group boundaries; (2) the token budget
 1313 assigned to each group by the allocator; and (3) the reconstructed mel-spectrogram obtained by
 1314 Gogo using only the allocated tokens. The visualization clearly demonstrates that the allocator
 1315 adaptively assigns more tokens to acoustically rich regions while reducing the allocation in silent or
 1316 low-information segments, thereby achieving efficient yet high-quality reconstruction.
 1317



1338
 1339 Figure 9: Visualization of sample 1580_141084_000085_000000 from the LibriTTS test-clean set.
 1340 The token allocator reduces the token rate from 47 Hz to 34.28 Hz.
 1341

M THE USE OF LARGE LANGUAGE MODELS

1342 Large language models were employed exclusively as auxiliary tools to edit and polish text written
 1343 by the authors. Their usage was limited to improving clarity, grammar, and style of expression. No
 1344 part of the research ideation, methodology, analysis, or results relied on LLMs.
 1345

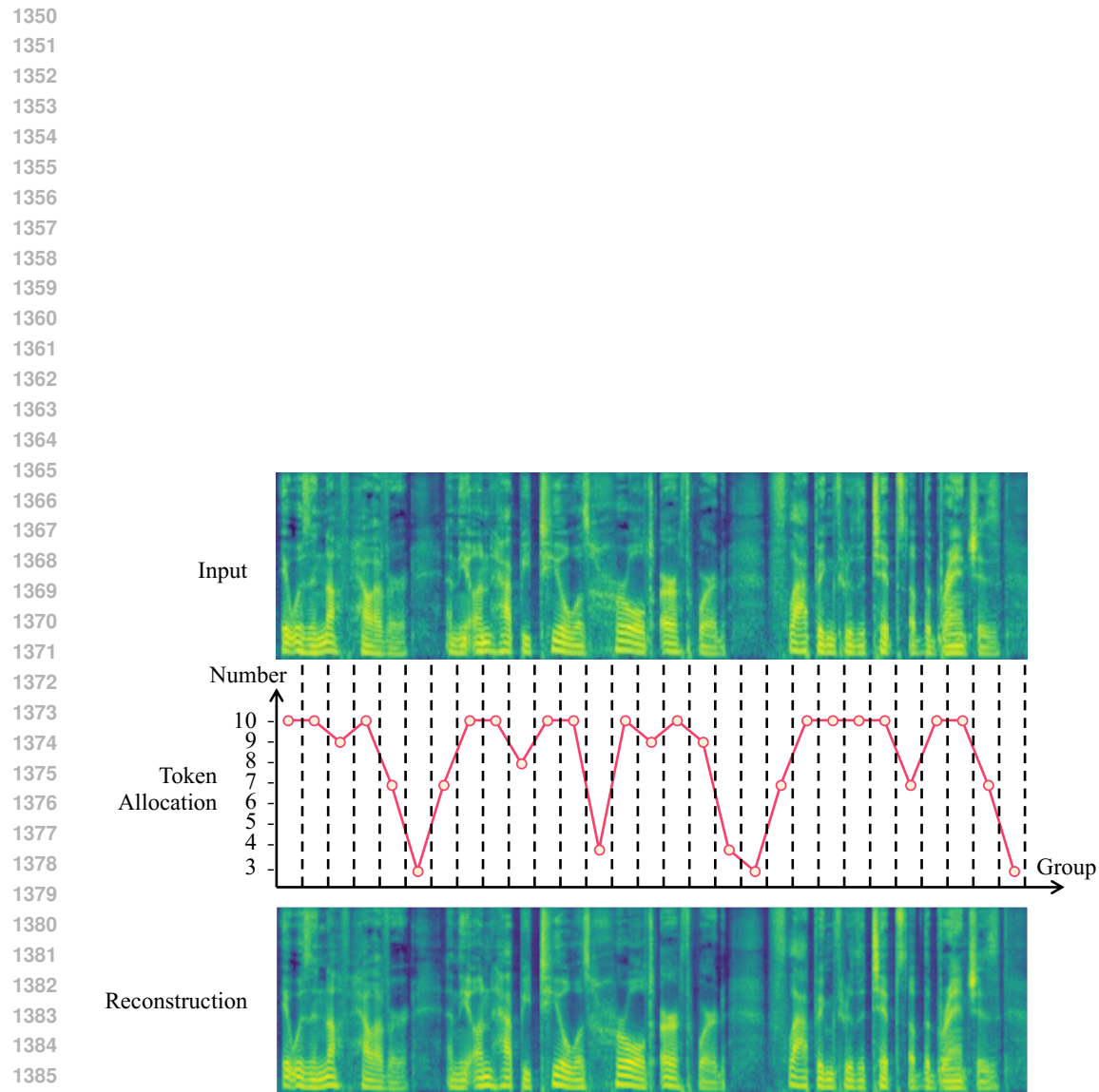


Figure 10: Visualization of sample 7176_88083_000011_000005 from the LibrtTTS test-clean set. The token allocator reduces the token rate from 47 Hz to 38.73 Hz.